THE ASTROPHYSICAL JOURNAL, 398:254–272, 1992 October 10

INFRARED EMISSION FROM DUST STRUCTURES SURROUNDING HERBIG Ae/Be STARS[1]

F. BERRILLI,[2] G. CORCIULO,[3] G. INGROSSO,[4] D. LORENZETTI,[5] B. NISINI,[5] AND F. STRAFELLA[3]

Received 1991 July 12; accepted 1992 April 6

ABSTRACT

We present IR observations in J, H, K, L, M, and 8–13 μm bands of Herbig Ae/Be stars located in the southern hemisphere. These results enlarge an already existing data base, increasing the significance of the correlations which can be obtained from observational parameters. Silicate features detected both in emission and in absorption indicate the presence of dust around these objects. A first analysis based on two-color diagrams, polarization, and luminosity suggests that the spherical geometry for the dust distribution is a more common feature, with respect to the flattened structure.

An emission model in which the central object is surrounded by a circumstellar envelope of gas and dust is introduced and the continuum spectrum is computed taking into account radiative properties both of gas (free-free, free-bound, electron scattering) and dust. The numerical results, compared with the observations, suggest that anisotropic dust distributions are not necessarily required to account for the emitting properties of the circumstellar envelopes around Herbig Ae/Be stars.

Subject headings: circumstellar matter — dust, extinction — stars: fundamental parameters — stars: pre–main-sequence

1. INTRODUCTION

The pre–main-sequence (PMS) nature of the Herbig Ae/Be stars is at present well established (see, e.g., Catala 1989). Consequently these objects are usually considered in connection with the lower mass T Tauri stars, with which they share the gross spectroscopic and photometric properties. However, when the "common" properties of these two classes of objects are investigated in more detail, some differences arise and the similarities become less compelling.

Among these, the significantly shorter Kelvin-Helmholtz time scales, the occurrence of a deuterium-burning shell beneath the photosphere (Palla & Stahler 1991), the greater projected rotational velocities (Finkenzeller 1985), and the magnitude of the optical variations exhibited by Herbig Ae/Be in comparison with T Tauri stars (Herbst, Holtzman, & Phelps 1982) all provide indication of important differences between the high- and low-mass PMS stars.

Moreover, as already noticed by Herbig (1960) in his original work, Ae/Be stars generally show a greater dispersion in the observed properties with respect to the more definite homogeneity exhibited by T Tauri stars. This behavior causes wider uncertainties in ascribing a specific property to the whole class, so that the statistical approach becomes a very important tool for studying the evolution of these intermediate mass-stars.

In this work we investigate the circumstellar (hereinafter CS) envelopes of the Herbig Ae/Be stars with particular emphasis on the geometry of the matter distribution. The relevance of this aspect is due to the fact that the capability to keep or to destroy flattened structures in the CS environment has a definite implication about the evolution of these stars toward the main sequence. In the case of T Tauri stars, e.g., where the presence of a disk has been supported both by theoretical predictions (e.g., Shu, Adams, & Lizano 1987 and references therein) as well as by many independent observational evidences (Strom et al. 1989; Cohen, Emerson, & Beichman 1989; Beckwith et al. 1990 and a list of less recent references therein), the disk itself may contribute significantly to, or even totally dominate, the energy output from these objects (e.g., Bertout 1989).

Similar definite conclusions lack for the more massive Herbig Ae/Be stars for which both spherical and flattened geometries have been invoked. Indirect indications for disks have been suggested for a dozen of Ae/Be stars (LkHα 198, Elias 1, V380 Ori, LkHα 208, R Mon, LkHα 25, Z CMa, R CrA, T CrA, V645 Cyg, LkHα 234, LkHα 233, and MWC 1080). These indications come from polarization maps (Warren-Smith et al. 1980; Shirt, Warren-Smith, & Scarrott 1983; Scarrott, Draper, & Warren-Smith 1989; Ward-Thompson et al. 1985; Lenzen 1987; Aspin, McLean & McCaughrean 1985), by measured line profiles (Edwards et al. 1987; Hamann & Persson 1989), by collimated mass outflows (Cantó et al. 1981; Rodríguez, Torrelles, & Moran 1981; Cantó et al. 1984; Levreault 1988; Sandell & Liseau 1985; Goodrich 1986; Poetzel, Mundt, & Ray 1989; Ray et al. 1990) and, finally, by biconical nebulae (Calvet & Cohen 1978). Other arguments have been suggested for LkHα 25 (Rydgren & Vrba 1987) and for Elias 1 (Kataza & Maihara 1991), the latter representing the first direct evidence, based on infrared speckle interferometry, for disk structure around an Ae star.

A systematic work to observe the millimetric dust emission and then to provide evidence of disks has been undertaken by Strom and collaborators, who recently presented their preliminary results for some intermediate-mass young stellar objects (Strom et al. 1991). They observed seven objects, four of which, namely LkHα 198, V594 Cas (otherwise BD +61154), KK Oph, and LkHα 234, are recognized members of (or candidates for) the Herbig Ae/Be class. However, due to the fact that LkHα 198 suffers confusion problems with the neighboring V376 Cas, which more likely possesses a CS disk (Leinert,

[1] Based in part on observations made at ESO (La Silla).

[2] Dipartimento di Fisica, Università di Roma "Tor Vergata," I-00133 Rome, Italy; also Istituto Fisica Spazio Interplanetario–CNR, Frascati, Italy.
[3] Dipartimento di Fisica, Università di Lecce, I-73100 Lecce, Italy; also Istituto Fisica Spazio Interplanetario–CNR, Frascati, Italy.
[4] Dipartimento di Fisica, Università di Lecce, I-73100 Lecce, Italy.
[5] Istituto Fisica Spazio Interplanetario–CNR, I-00044 Frascati, Italy.

Haas, & Lenzen 1991), and that LkHα 234 is located in a region of spatially extended emission, we can speak of unambiguous detection only for KK Oph and BD +61154. In the same paper, using the relation given by Adams, Emerson, & Fuller (1990), the authors also provide a rough estimate of the upper limit of the disk mass (0.01 $M_\odot$ for KK Oph and 0.3 $M_\odot$ for BD +61154) that, due to the uncertainties on grain emissivity and disk temperature, should be considered uncertain at least for a factor of 10.

This determination led them to favor a disk distribution for the dust because, if this mass were distributed in a spherical region with dimension determined assuming a thick envelope at 60 μm, these objects would be optically invisible. However, this assumption appears questionable both because it implies an envelope necessarily thicker at visual wavelengths and because it is in striking contrast with the very low optical depth at 100 μm derived by Natta et al. (1992) by fitting the overall energy distribution observed in LkHα 198.

The aforementioned difficulties give us the feeling that we are still far from reaching definite conclusions on the dust geometry as inferred from visual extinction.

The controversy on the matter distribution around intermediate-mass young stars emerges more clearly when we consider that, by exploiting independent methods, opposite conclusions have been reached for some of the objects listed above. In fact, near-IR speckle interferometry provides indication for a spherical structure around LkHα 198 (Leinert et al. 1991) and spatial scans on the same 50 μm and 100 μm are in favor of a spherical symmetry (Natta et al. 1992). In the last case, however, to explain the overall energy distribution, and in particular the near-IR, a disk combined with a spherical envelope, or alternatively a pure spherical envelope including very small grains, has been invoked.

Early FIR observations (Harvey, Thronson, & Gatley 1979) including LkHα 198, V380 Ori, R Mon, MWC 1080, have been interpreted in terms of a spherical dust shell with $\rho(r) \propto 1/r$ density distribution, and more recent numerical radiative transfer codes, used to explain the far-UV to far-IR energy distribution of the prototype object AB Aur, confirm the spherical geometry (Sorrell 1990).

Other examples of these difficulties come from the work of Bastien & Menard (1990) who point out that sources with a centrosymmetric pattern in their polarization maps, such as V380 Ori and LkHα 208, not necessarily must be surrounded by an optically thick disk. This is because single scattering in an optically thin spherical dust distribution also provides such a pattern. Moreover, indication of a dust ring around LkHα 234 comes from the submillimeter maps of Dent et al. (1989) so as the absence of mid-IR with respect to the near-IR and submillimeter emission has been interpreted by Bechis et al. (1978) as due to a spherical dust distribution.

Finally, at variance with the T Tauri stars, a strong indication favoring a spherical geometry is the observation in the Herbig Ae/Be stars of a symmetric profile in the [O I] line at 6300 Å together with a reduced Balmer excess (Catala 1989).

The presence of disks is however of primary evolutionary significance and the fact they have been detected in highly luminous young stellar objects of the kind of S106 IRS 3 and GL 490 (Persson, McGregor, & Campbell 1988) as well as in main-sequence A stars like α Lyr and β Pic (Aumann et al. 1984; Smith & Terrile 1984; Paresce & Burrows 1987) must be considered. This is because these objects can be thought of, respectively as progenitors of and successors to the Herbig Ae/Be stars, even if some doubts could be raised on the evolutionary link with the former, that could be merely higher mass objects. It is difficult, however, to quantify the importance of this disk in determining the IR emission at the stage of the Herbig Ae/Be stars because we do not know when and how an initially massive disk ($\sim 1\ M_\odot$) evolves in a much lighter structure ($\sim 10^{-6}\ M_\odot$) as observed in α Lyr and β Pic.

In this paper we present new infrared observations which allow us to derive in § 2 the dust temperature ($T_{\rm dust}$) and optical depth ($\tau_{9.7\,\mu m}$), while in § 3 the catalog of the *IRAS* fluxes is given and the selection criteria are discussed. In § 4 we analyze the bolometric luminosities of the Herbig Ae/Be stars and how their position in the Hertzsprung-Russell (H-R) diagram is related to the observed properties. In § 5 a model is presented to compute synthetic spectra emerging from CS envelopes of young stars. The correlations between observed parameters and the comparison of our numerical results with the observations are discussed in § 6.

2. OBSERVATIONS AND RESULTS

The observations were carried out in 1989 April at the 1 m ESO telescope (La Silla, Chile), equipped with an InSb detector (*J*, *H*, *K*, *L*, and *M* bands) and a Ge-Ga bolometer (*N*1, *N*2, *N*3 bands). The filter characteristics and the absolute flux calibration are given by Bouchet, Manfroid, & Schmider (1991). We used a focal plane aperture and E/W chopping throw of 15″ and 27″, respectively.

In the 10 μm region, multiple observations of the program stars were made on different nights allowing us to give uncertainties for the *N*1, *N*2, *N*3 photometry, accounting both for intrinsic errors (statistical, zero-point calibrations, atmospheric extinction) and for the reproducibility of the observed magnitudes.

Two northern Ae/Be stars have also been observed (1990 July) in the near-IR, at the 1.5 m Italian IR telescope at Gornergrat (CH), and the obtained magnitudes are reported for completeness.

The overall results are presented in Table 1, which gives the magnitudes (*J*, *H*, *K*, *L*, *M*, *N*2) and the color indices ([*N*1 − *N*2], [*N*2 − *N*3]), used to evaluate the occurrence, in emission or absorption, of the silicate feature (at 9.7 μm). The relationship between the observed colors and the physical parameters, namely temperature ($T_{\rm dust}$) and optical depth ($\tau_{9.7}\,\mu$m) of the CS dust envelope, is established using the model described in a previous paper (Berrilli et al. 1987, hereafter Paper I). However, two minor modifications are here introduced:

1. The optical efficiency $Q(\lambda)$ for the silicate grains (assumed to be 0.01 μm in size), is now taken from Draine & Lee (1984).

2. Since the effective wavelength of each filter varies with the spectral shape of the incident flux $E(\lambda)$, we introduce a new effective wavelength $\lambda_{\rm eff}$ defined by

$$\lambda_{\rm eff} = \frac{\int \lambda E(\lambda) S(\lambda) d\lambda}{\int E(\lambda) S(\lambda) d\lambda}\,, \tag{1}$$

where $S(\lambda)$ is the instrumental response function, assumed coincident with the filter response. The last modification affects mainly the *N*1 and *N*3 bands because they fall on the wings of the silicate feature, where the spectral slope is rapidly changing with the wavelength.

The model results, calculated for selected values of $\tau_{9.7\,\mu m}$ and $T_{\rm dust}$, are shown, as a grid, in the two-color diagram of

TABLE 1

IR PHOTOMETRY OF SOUTHERN HERBIG Ae/Be STARS

A. OBSERVATIONS

Number[a]	Source	J	H	K	L	M	$N2$	$[N1-N2]$	$[N2-N3]$
25	CoD −443318	8.08	6.96	5.87	4.27	3.85 (5)	...	...	...
26	HD 76534	7.64	7.58	7.42	7.36 (30)	>7.4	...	...	...
27	RCW 34	9.24	8.84	8.54	...	...	...	...	...
28	RCW 36	8.34	7.19	6.57	6.19 (12)	6.88 (50)	...	...	...
29	Herbst 28	9.59	9.22	9.07	...	...	...	...	...
30	HD 97048	7.40	6.89	6.22	4.80	4.68 (16)	2.53 (8)	−0.51	1.42
31	HR 5999	5.73 (3)	5.07	4.25	2.91	2.55 (3)	0.97	0.22	0.24
32	HD 150193	7.02 (3)	6.28	5.47	4.23 (3)	3.93 (6)	0.97	0.83	0.01
33	CoD −4211721	7.36 (3)	5.98	4.51	2.38	1.75	0.23 (11)	−0.03	0.58
34	KK Oph	8.52	6.99	5.64	3.97 (4)	2.59 (20)	1.37	0.58	0.15
35	HD 163296	6.28 (3)	5.58	4.72	3.50	3.18 (3)	0.69	0.74	0.05
36	LkHα 118	8.88 (3)	8.40	7.99	7.54 (31)	>6.5	...	...	...
37	LkHα 119	9.83 (3)	9.40	9.04	8.30 (32)	>6.5	...	...	...
38	MWC 297	6.35 (3)	4.63	3.19	1.23	0.58	−1.17 (9)	0.11	0.64
39	VV Ser	8.77 (3)	7.47	6.32	4.81 (3)	4.34 (7)	2.38 (18)	0.72	0.65
40	MWC 300	9.29 (3)	8.20	6.19	2.79	1.77	−0.57	0.17	0.74
41	AS 310	10.34	10.03	9.48	7.39 (23)	>6.6	2.45 (13)	0.18	0.59
42	TY CrA	7.56	7.02	6.70	6.23 (4)	6.56 (19)	2.72 (9)	−0.78	1.41
43	R CrA	7.53	5.41	3.63	1.48	0.93	−0.97 (8)	0.41	0.52
44	T CrA	9.25	7.75	6.44	4.76	4.31 (5)	2.35 (15)	0.27	0.75
55	HD 216629	7.25 (3)	6.84	6.36	6.69 (8)	...	...	...	...
56	BHJ 71	8.44 (3)	7.97	7.55	6.99 (3)	...	...	...	...

B. FILTER CHARACTERISTICS[b]

Parameter	J	H	K	L	M	$N2$	$N1$	$N3$
λ_{eff} (μm)	1.23	1.63	2.19	3.79	4.64	9.69	8.38	12.89
Zero magnitude flux (watt cm^{-2} μm^{-1})	3.24×10^{-13}	1.26×10^{-13}	4.20×10^{-14}	5.22×10^{-15}	2.44×10^{-15}	1.12×10^{-16}	2.08×10^{-16}	3.55×10^{-17}

NOTE.—Errors given in parentheses are expressed in units of 10^{-2} mag whenever they exceed 0.02 mag. The errors in the colors $[N1-N2]$, $[N2-N3]$ are shown in Fig. 1.

[a] List number given by Finkenzeller & Mundt 1984.

[b] Effective wavelength and the zero magnitude corresponding flux for each filter are reported.

Figure 1. In the same figure the observed colors, also given in Table 1, are superposed. No reddening correction has been applied because both the intrinsic low value of the relative extinction $A(\lambda)/A_V$ (see Rieke & Lebofsky 1985), and the spectral vicinity of the three filters.

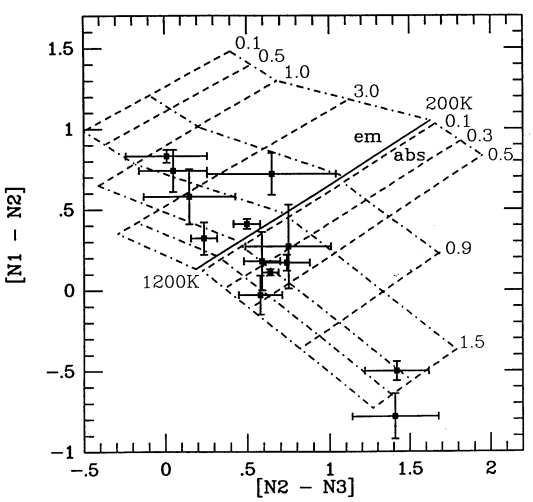

FIG. 1.—$[N1-N2]$, $[N2-N3]$ color plot for the observed Ae/Be stars. The dash-dotted lines correspond to different dust temperatures (200, 300, 400, 600, 800, and 1200 K), while the dashed lines correspond to different optical depths in emission or absorption. The solid line represents the blackbody line.

As in Paper I, when the error box associated with a source includes the blackbody line we consider the source featureless (BB). In the other cases, we distinguish between silicate emission (E) and silicate absorption (A). The resulting assignment, as well as the derived dust temperature and optical depth at 9.7 μm, are listed in Table 2 (BB denotes the absence of any feature). As a comparison, the identification of the same feature obtained by different authors is given. For the sake of homogeneity, we reconsider our previous observations (Paper I), adopting the two modifications (1) and (2) described above. The results reported at the bottom of Table 2 show that the discrepancies with Paper I are always less than 20%, thus leaving unaffected our previous conclusions.

In order to enlarge our sample, we preferred the filter photometry ($N1$, $N2$, $N3$) instead of CVF spectrophotometry, because the narrower CVF bandpass impose a higher flux limit. Nevertheless, three out of the brightest objects (CoD −4211721, MWC 297, and R CrA) have been also observed in the 8–13 μm range, with the CVF at low equivalent resolution ($R = 20$).

During the acquisition of the CVF spectra, the standard star HR 6134 (α Sco) was repeatedly observed in the $N1$, $N2$, $N3$ filters, to check the stability of the zero points. These remained constant, within 0.02 mag, during the measurements. Moreover, because the standard star showed blackbody colors at these wavelengths, all the spectra have been reduced assuming that HR 6134 radiates as a blackbody at a temperature of 3600 K (spectral type M1 I).

TABLE 2

SILICATE FEATURES IN HERBIG Ae/Be STARS

Number[a]	Source	Feature[b]	T_D[c] (K)	$\tau_{(9.7\ \mu m)}$[d]	Other Observations[b] 8–13 μm and References[e]
30	HD 97048	A	600	1.4	A (1); E (11.25) (2, 3)
31	HR 5999	BB	700	...	Flat (1)
32	HD 150193	E	350	1.2	E (1, 4)
33	CoD −4211721	A	900	0.5	
34	KK Oph	E	500	3.0	
35	HD 163296	E	400	1.8	E (1, 5)
38	MWC 297	A	650	0.4	Flat (?) (6)
39	VV Ser	BB	350	...	
40	MWC 300[f]	A	550	0.4	Flat (1)
41	AS 310	BB	600	...	E (7)
42	TY CrA	A	1050	1.7	E (11.05, 11.25) (3)
43	R CrA	BB	500	...	Flat (?) (8) E (6)
44	T CrA	BB	450	...	Flat (?) (8)
1	LkHα 198	E	200	1.5	E (1), flat (6)
2	BD +61154	E	300	1.5	E (5)
5	AB Aur	E	500	0.4	E (1, 5, 9)
6	HK Ori	A	350	0.7	
8	T Ori	A	500	0.8	
9	V 380 Ori	E	400	1.5	E (9)
13	HD 250550	BB	200	...	E (9)
17	HD 259431	A	750	0.3	A (1), flat (5)
22	Z CMa	A	450	0.7	A (9), flat (5)
49	HD 200775	A	450	0.4	
52	LkHα 234	A	450	0.3	
54	LkHα 233	E	400	0.3	
57	MWC 1080	BB	500	...	A (1, 9)

[a] List number given by Finkenzeller & Mundt 1984.

[b] Occurrence of silicate absorption (A) or emission (E) with BB denoting the absence of any feature.

[c] Derived dust temperature.

[d] Optical depth at 9.7 μm.

[e] Other observations made by different authors in the same spectral range, are reported for comparison.

[f] The source MWC 300 (number 40) is included in this list (but not in the following analysis) only for completeness, because it is recognized as an evolved star (B1 hypergiant according to Wolf & Stahl 1985).

REFERENCES.—(1) IRAS-LRS 1986. (2) Aitken & Roche 1981. (3) Roche, Aitken, & Smith 1991. (4) Elias 1978a. (5) Sitko 1981. (6) Volk & Cohen 1989. (7) Cohen 1974. (8) Vrba, Strom, & Strom 1976. (9) Cohen & Witteborn 1985.

The CVF observations are shown in Figure 2, where the error bars account for the statistical error (one standard deviation) due to integration on the source. The solid lines represent profiles obtained using values of T_{dust} and $\tau_{9.7\ \mu m}$ derived by the filter photometry (see Table 2). The agreement is satisfactory and provides a direct proof of the reliability of this approach.

Finally, to fully account for the existing data in the $N1$, $N2$, and $N3$ photometric bands, we computed T_{dust} and $\tau_{9.7\ \mu m}$ for eight sources whose fluxes are available in literature. The results are given in Table 3, but demand some caution because they come from inhomogeneous data sets (see notes to Table 3).

3. *IRAS* FLUXES

Since the dust is certainly associated to the Herbig Ae/Be stars, it is worthwhile to search for *IRAS* counterparts of these objects, obtaining photometric data between 12 and 100 μm, which elucidate about the dust emission down to a few tens of kelvins. Moreover, some of the spectral energy distributions derived from near-IR observations of the Herbig Ae/Be stars,

TABLE 3

SILICATE FEATURE IN HERBIG Ae/Be STARS

Number[a]	Source	Feature	T_D (K)	$\tau_{(9.7\ \mu m)}$	Reference
3	XY Per[b]	...	...	...	1
4	Elias 1	E	250	2.2	2
12	HD 37490	BB	2000	...	3
14	LkHα 208	E	500[c]	0.12[c]	4
18	R Mon	BB	450	...	4
19	LkHα 25	BB	500	...	5
45	BD +404124[b]	...	...	...	6
50	V645 Cyg	A	400	1.1	7

[a] List number given by Finkenzeller & Mundt 1984.

[b] The authors used an $N2$ filter ($\lambda_0 = 10.8$ μm) which is more displaced toward the red when compared with those usually employed; thus, it could originate some uncorrect interpretation about the occurrence of emission or absorption feature.

[c] Given parameters are computed by the authors themselves.

REFERENCES.—(1) Cohen 1973a b. (2) Elias 1978b. (3) Gehrz, Hackwell, & Jones 1974. (4) Cohen & Witteborn 1985. (5) Rydgren & Vrba 1987. (6) Cohen 1972. (7) Lebofsky et al. 1976.

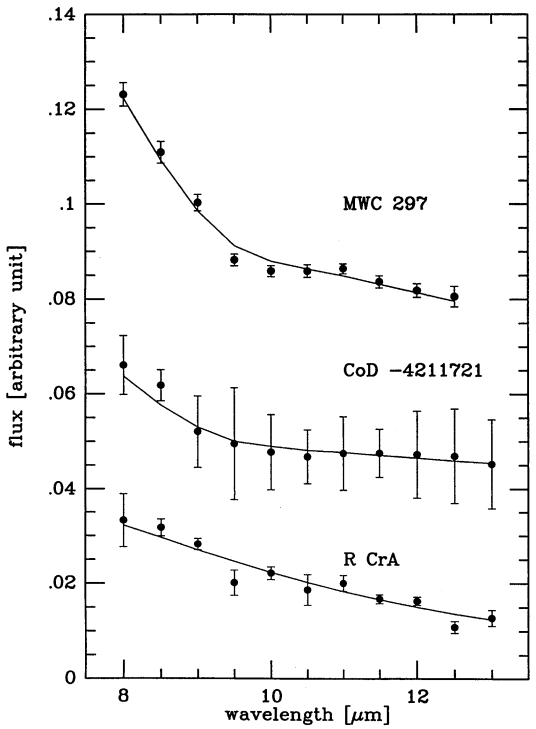

FIG. 2.—Low-resolution CVF spectra of R CrA, CoD −4211721, and MWC 297 in the range 8–13 μm. Solid lines represent the $F(\lambda)$ profiles derived from the $N1$, $N2$, $N3$ photometry of the same objects (see text).

seem to peak at greater wavelengths, where substantial contributions may arise to the bolometric luminosities.

We adopted as primary data base the catalog of 57 Herbig Ae/Be stars given by Finkenzeller & Mundt (1984) which includes the 26 stars compiled by Herbig (1960). We then searched for PSC (Point Source Catalog, Version 2; Beichman et al. 1985) *IRAS* counterparts whose spatial uncertainty ellipses (95% confidence level) included the optical identification. Only fluxes of quality 3 or 2 (the latter occurring in very few cases) were considered, excluding upper limit detections. In particular, the 100 μm flux was recognized only for sources with a cirrus contamination less than 20% (C2 flag <4).

Since we consider the spatial coincidence as the main criterion for the association, we adopted the most accurate determinations of the optical/near-IR position of each star. The coordinates were taken from the Third Catalog of Emission Line Stars of the Orion Population by Herbig & Bell (1988) with the exception of the following stars: HD 37490, HD 52721, HD 150193, HD 163296 (SAO Catalog); RCW 34, Herbst 28, HD 76534 (Herbst 1975); RCW 36 (Braz & Epchtein 1982); LkHα 119 (Herbig 1957); MWC 297 (Allen et al. 1977); LkHα 134 (Herbig 1958); V 645 Cyg (Gezari, Schmitz, & Mead 1987); HD 216629, BHJ 71 (Blaauw, Hiltner, & Johnson 1959).

Following the above criteria, 30 sources, given in Table 4A, have been selected, and they form our primary list of identifications. Four additional sources of Table 4, namely LkHα 25, HD 97048, MWC 297, and CoD −443318, were selected out of 14 objects that do not meet the criterion for the spatial coincidence, but lie inside a box of 1 arcmin^2 centered on the optical position. For the first three objects, the N-band (10 μm) ground-based photometry is available, and the selection criterion has been the comparison between the N magnitude and the 12 μm *IRAS* flux. In this respect we defined the parameter A

$$A = \log \frac{\nu F(\nu)_{\rm IRAS}}{\nu F(\nu)_{\rm ground\text{-}based}}, \qquad (2)$$

and because the 30 primary identifications have $|A| < 0.5$, we assumed this value as a selection criterion. Finally, for the last additional source (CoD −443318), for which no N magnitude is available, we adopted a further criterion based on the spectral index

$$\alpha_{1,2} = \frac{\log (F_{\nu_1}/F_{\nu_2})}{\log (\nu_1/\nu_2)}.$$

This source has been selected by requiring that

$$\alpha_{L,M} = \alpha_{L,12\ \mu\rm m} \pm 0.2$$

to ensure a continuous spectrum and

$$\alpha_{L,M} = \alpha_{12\ \mu\rm m,25\ \mu m} \pm 0.2$$

to have the same spectral index between L and 25 μm.

These 34 identifications are reported in the first part of Table 4A and in the following will be referred to as the "most probable identifications." For completeness, we list at the bottom of the same table six more sources for which the previous selection criteria were inapplicable due to the absence of ground-based data. The angular distance from the optical position is given for each of them, and we shall refer to these sources merely as "probable identifications."

Once the *IRAS* counterparts have been selected, their compactness coefficients (CC flag in the *IRAS*-PSC), expressed as percentage from 100% (A) to 87% (N) (Beichman et al. 1985), are considered. These indicate the pointlike nature of the source in each *IRAS* band with respect to the instrumental response.

The most probable identifications seem largely pointlike sources because 20 of them have a type A coefficient for all the bands, while the remaining sources (five with A and B, six with ABCD, and only three with some EF) possess type A coefficients for more than 50% of the detected bands. The same conclusion does not apply for the last six sources of Table 4A, for which the A coefficient is not frequently seen (only four occurrences out of 17 detected bands).

After we have reliable *IRAS* identifications, we can use the observed fluxes to draw a two-color diagram for these stars. As *IRAS* color $(\lambda_1 - \lambda_2)$ we define $\log [F_\nu(\lambda_2)/F_\nu(\lambda_1)]$, where $F_\nu(\lambda)$ is the flux density (in Jy) in the wavelength band centered on λ (in μm). Such a diagram is shown in Figure 3 in which we note preliminarily that the stars recognized as "probable identifications" are listed at the bottom of Table 4A, show different colors when compared with the bulk of the "most probable identifications," confirming the uncertainty of their association. From Figure 3 it is also evident that the *IRAS* spectra of the Herbig stars are not consistent with a single blackbody, but can be described in terms of different dust components with temperature ranging between 70 and 170 K. Furthermore their *IRAS* colors are more scattered with respect to the locus (*hatched area*) defined by a significant number (116) of classical T Tauri stars, as given by Weintraub (1990).

Finally it is worth noting that, for the Herbig stars, a significant dispersion exists around the value −0.13 of the [25−60] index. This value corresponds to the spectral slope expected for an accretion or reprocessing CS disk, thus suggesting that we

TABLE 4A

IRAS COUNTERPARTS OF HERBIG Ae/Be STARS

NUMBER[a]	SOURCE	*IRAS* IDENTIFICATION[b]	FLUX DENSITY[c] (Jy) 12 μm	25 μm	60 μm	100 μm	ANGULAR DISTANCE
1	LkHα 198	00087+5833	33.0	88.1	127	183	
2	BD +61154	00403+6138	7.39	9.13	5.15	...	
3	XY Per	03462+3849	3.85	4.06	4.91	...	
4	Elias 1	04155+2812	33.2	99.9	72.7	168	
5	AB Aur	04525+3028	27.2	48.1	106	114	
6	HK Ori	05286+1207	3.79	4.08	...	...	
7	BD +9880	05324+0959	4.00	5.96	4.97	...	
9	V380 Ori	05339−0644	8.61	8.85	...	...	
10	BF Ori	05348−0636	0.96	0.80	...	...	
11	RR Tau	05363+2620	1.74	2.20	4.46	36.7	
12	HD 37490	05365+0405	1.21	0.58	...	...	
13	HD 250550	05591+1630	4.53	9.87	7.27	10.6	
14	LkHα 208	06048+1839	3.39	3.99	5.60	...	
17	HD 259431	06303+1021	12.5	20.2	109	159	
18	R Mon	06364+0846	54.7	132	121	149	
19	LkHα 25	06299+1011	9.13	9.29	...	...	
21	LkHα 218	07003−1121	0.73	...	...	...	
22	Z CMa	07013−1128	127	221	322	354	
23	LkHα 220	07017−1121	1.62	2.10	...	...	
25	CoD −443318	07178−4429	6.68	7.60	13.1	33.6	
30	HD 97048	11066−7722	14.5	40.3	69.9	...	
31	HR 5999	16052−3858	18.0	14.5	14.4	...	
32	HD 150193	16372−2347	17.6	18.1	8.13	...	
33	CoD −4211721	16555−4237	94.9	252	1918	2213	
34	KK Oph	17070−2711	9.87	9.56	6.14	...	
35	HD 163296	17533−2156	18.2	21.0	28.2	...	
38	MWC 297	18250−0351	159	224	914	1803	
39	VV Ser	18262+0006	4.61	3.77	6.33	24.3	
41	AS 310	18306−0500	24.4	93.3	685	1309	
43	R CrA	18585−3701	111	221	608	1206	
50	V645 Cyg	21381+5000	114	219	371	455	
53	BD +463471	21505+4659	1.59	1.67	2.60	...	
55	HD 216629	22513+6152	2.70	2.30	...	...	
57	MWC 1080	23152+6034	22.2	25.1	147	...	
15	MWC 137[d]	06158+1517	9.67	22.9	234	337	13″
20	HD 52721[d]	06594−1113	1.41	4.43	...	...	18
24	HD 53367[d]	07020−1022	2.15	21.0	...	...	13
26	HD 76534[d]	08533−4316		0.71	...	...	27
27	RCW 34[d]	08546−4254	29.3	194	1343	2098	11
28	RCW 36[d]	08566−4313	0.52	0.30	7.86	20.7	24

[a] List number given by Finkenzeller & Mundt 1984.
[b] *IRAS* name.
[c] Color-uncorrected flux densities in Jy.
[d] Probable *IRAS* associations (see text) together with angular distance from the optical positions.

TABLE 4B

KAO (50 μm) FLUXES OF HERBIG Ae/Be STARS

Number[a]	Source	50 μm Flux (Jy)	Aperture	Reference	[Q−50][b]	[25−60][b]
1	LkHα 198	80 (52 μm)	37″	1	0.78	0.16
9	V380 Ori	15	45	2	0.29	...
14	LkHα 208	<5	...	3	<−0.01	0.15
18	R Mon	81 (52 μm)	37	1	−0.05	−0.04
22	Z CMa	390	45	2	0.31	0.16
42	TY CrA	145	45	4	1.20	...
43	R CrA	290	45	4	0.14	0.44
50	V645 Cyg	290	...	3	0.26	0.23
52	LkHα 234	390 (53 μm)	37	5	1.28	...
54	LkHα 233	24	45	2	0.42	...
57	MWC 1080	87 (52 μm)	37	1	0.82	0.77

[a] List number given by Finkenzeller & Mundt 1984.
[b] The [Q−50] and the *IRAS* [25−60] color indices are obtained from observations carried out with different apertures, typically 20″–40″ for the former and 45″–90″ for the latter.

REFERENCES—(1) Harvey, Thronson, & Gatley 1979. (2) Evans, Levreault, & Harvey 1986. (3) Harvey & Wilking 1982. (4) Wilking et al. 1985. (5) Bechis et al. 1978.

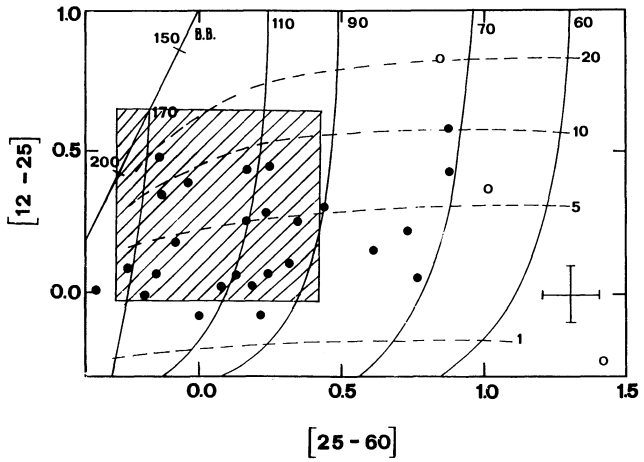

FIG. 3.—The *IRAS* two-color diagram of the Herbig Ae/Be stars according to the fluxes given in Table 3. Different symbols indicate the "most probable" (*filled circles*) and the "probable" identifications (*open circles*). Solid curves represent the sum of two blackbodies, one at 1000 K and the other at the indicated temperature. The ratio at 25 μm of the two contributions is also shown as dashed lines labeled by the relative percentage. The straight line indicates the colors of a single blackbody at different temperatures. The hatched area indicates the locus of the classical T Tauri stars (see text), and the cross represents the mean error in color.

cannot describe the *IRAS* spectra of the Herbig stars as emitted by simple disk structures around the central object. However, because the observations at 25 and 60 μm are obtained with beam sizes of 45″ and 90″, respectively, a brief discussion is in order about the possibility that the dispersion in Figure 3 could find an alternative explanation as a result of sources confusion or extent.

In this respect, we can compare the *IRAS* fluxes with ground-based and KAO observations which are carried out at wavelengths close to the *IRAS* ones but typically with smaller apertures. In this way, a plot of the available N fluxes versus the *IRAS*-PSC ones at 12 μm has shown a weak beam size effect, while a similar plot for the Q band versus the 25 μm *IRAS* fluxes suggests that such an effect is present. At longer wavelengths a comparison between *IRAS* and KAO observations at 50 μm (see, e.g., Tables 4A and 4B) evidences that, in most cases, the *IRAS* fluxes at 60 μm are to be considered an upper limit to the true stellar flux, the same trend being even more evident at 100 μm.

If we now examine the color $[25-60]$, we note that our sources are evaluated by *IRAS* as pointlike (see discussion in § 3) at both wavelengths so that the source's extent should not be the cause of the scatter observed in Figure 3. On the other hand, to obtain an indication on the possibility of sources confusion, we can use the ground-based and KAO fluxes, obtained with smaller apertures (typically 10″–40″, respectively), to derive the color index $[Q-50]$ that is the closer alternative to the *IRAS* $[25-60]$ color index. In Table 4B the KAO data available in the literature are summarized along with the derived values for the $[Q-50]$ color index and the *IRAS* $[25-60]$ color index, the latter reported for comparison.

It is apparent that the dispersion in the $[Q-50]$ is not reduced with respect to that in the $[25-60]$ index. In fact, if we consider only the six objects for which both KAO and *IRAS* data are available we have for the average colors $\langle[25-60]\rangle_{6\text{obj}} = 0.27 \pm 0.26$ and $\langle[Q-50]\rangle_{6\text{obj}} = 0.30 \pm 0.31$ while, including all the detected sources we obtain $\langle[25-60]\rangle_{\text{all}} = 0.21 \pm 0.33$ and $\langle[Q-50]\rangle_{\text{all}} = 0.47 \pm 0.43$, the latter being even more discrepant and dispersed with respect to the value -0.13 expected for a disk.

Therefore we are left with the possibility that the sources are extended at the scale of the ground-based and KAO observations. This would account for the higher fluxes observed by *IRAS*, but, because of the sizes involved at the distances of the Herbig Ae/Be stars, it prevents any definite conclusion on the genuine meaning of the scatter in the color diagram.

It is noteworthy, however, that, despite an increase in spatial resolution by using ground-based and KAO observations, the scatter in the color index persists.

4. LUMINOSITIES

Once the *IRAS* fluxes of the Herbig Ae/Be stars are known, it is possible to obtain their composite energy distributions with the aim of reexamining the bolometric luminosities considered to this point and to discuss their location in the H-R diagram.

Before computing bolometric luminosities we should have defined the dust geometry because the presence of a disk (active or passive) could substantially alter the estimate of the luminosity by adding contributions due to accretion and/or geometrical effects (Kenyon & Hartmann 1987). However, because the mass accretion rate as well as the disk inclination are usually unknown, here the luminosities will be derived under the assumption of isotropic emission so that they should be considered as upper limits to the true stellar luminosity.

The visual and infrared data we considered to evaluate the bolometric luminosities are reported in the Appendix. We are aware that the data presented in Table 8 are not always uncontroverted and that for some objects substantial uncertainties exist. However, the criterion we used in compiling this table has been to favor the source papers which provide the more homogeneous data set in order to minimize any inconsistency among the derived quantities. In any case, the large sample used should ensure that systematic errors in deriving the physical quantities (e.g., luminosities) are avoided and that the consequent conclusions, which are statistical in nature, are not critically dependent on some unavoidable discrepancies occurring in individual objects.

Since it is not straightforward to disentangle the CS from the interstellar contributions to the extinction for each object, we compute two different luminosities L_{min} and L_{max} as in Finkenzeller & Mundt (1984). These luminosities respectively stem from the position to ignore the interstellar extinction in favor of the CS contribution alone and vice versa. To calculate L_{max}, optical and near-IR magnitudes (from U to N) have been dereddened using the Rieke & Lebofsky (1985) extinction law, while no correction was applied both to the Q magnitudes, and to the *IRAS* fluxes. On the other hand, L_{min} values were obtained without applying any correction to the observed energy distributions. Both L_{min} and L_{max} include the contributions from U to 100 μm and an additional term L_{corr} which accounts for contributions at longer wavelengths (Cohen 1973d; Chavarria-K. 1981). Table 5 lists these luminosities as well as the individual contributions due to the *IRAS* fluxes and to the correction term. The contributions to the luminosity shortward of 0.36 μm can be derived for a very limited number of stars (Sitko 1981; Thé et al. 1986) but are not considered here, amounting typically to a few percent of the bolometric luminosity. On the other side, for wavelengths longer than 100

TABLE 5

LUMINOSITY COMPONENTS FOR THE HERBIG Ae/Be STARS

Number[a]	Source	$L_{min}/L_{\odot}$[b]	$L_{max}/L_{\odot}$[c]	$L_{IRAS}/L_{\odot}$[d]	$L_{corr}/L_{\odot}$[e]
1	LkHα 198	3.40E+02	5.60E+02	2.12E+02	7.04E+01
2	BD +61154	1.52E+02	3.36E+02	2.69E+01	3.87E+00
3	XY Per	9.99E+00	1.99E+01	8.11E−01	2.24E−01
4	Elias 1	2.07E+01	5.60E+01	1.13E+01	3.35E+00
5	AB Aur	5.78E+01	7.96E+01	1.01E+01	3.12E+00
6	HK Ori	2.73E+01	4.05E+01	4.06E+00	3.69E+00
7	BD +9880	2.91E+01	3.95E+01	6.22E+00	1.42E+00
8	T Ori	4.41E+01	7.45E+01	...	6.78E+00, 1.15E+01
9	V380 Ori	8.37E+01	1.36E+02	9.12E+00	8.00E+00
10	BF Ori	2.03E+01	3.19E+01	9.80E−01	7.23E−01
11	RR Tau	1.08E+02	3.46E+02	1.62E+01	2.51E+01
12	HD 37490	1.85E+03	2.77E+03	7.05E−01	3.21E−01
13	HD 250550	1.44E+02	1.63E+02	2.99E+01	5.55E+00
14	LkHα 208	3.35E+02	5.85E+02	1.20E+02	3.99E+01
15	MWC 137	7.50E+02	7.50E+02	3.22E+02	2.92E+02
16	LkHα 215	2.79E+02	6.91E+02	...	5.58E+00
17	HD 259431	6.03E+02	1.05E+03	1.60E+02	1.09E+02
18	R Mon	1.16E+03	1.66E+03	5.22E+02	1.02E+02
19	LkHα 25	6.65E+01	8.60E+02	2.92E+01	2.54E+01
20	HD 52721	2.79E+03	6.07E+03	1.30E+01	2.50E+01
21	LkHα 218	6.64E+01	9.27E+01	...	8.59E+00
22	Z CMa	6.36E+03	1.01E+04	2.17E+03	5.00E+02
23	LkHα 220	6.85E+01	8.38E+01	1.13E+01	1.19E+01
24	HD 53367	2.36E+03	1.80E+04	3.74E+01	1.19E+02
25	CoD −443318	8.61E+01	8.81E+01	1.45E+01	7.27E+00
26	HD 76534	3.67E+02	8.96E+02	...	2.30E+00
27	RCW 34	3.58E+03	5.23E+03	1.83E+03	1.70E+03
28	RCW 36	1.14E+02	1.14E+02	1.42E+01	2.21E+01
29	Herbst 28	2.97E+01	3.68E+02	...	5.86E+00, 8.07E+00
30	HD 97048	1.75E+01	3.11E+01	5.13E+00	2.80E+00
31	HR 5999	1.64E+02	1.82E+02	9.44E+00	1.87E+00
33	CoD −4211721	1.12E+03	6.43E+03	5.51E+02	3.78E+02
34	KK Oph	5.41E+01	1.35E+02	7.26E+00	1.05E+00
35	HD 163296	4.30E+01	5.19E+01	3.56E+00	1.13E+00
36	LkHα 118	2.10E+02	2.94E+03	...	2.46E+01, 2.99E+01
37	LkHα 119	8.14E+01	6.51E+02	...	1.22E+01, 1.45E+01
38	MWC 297	1.61E+03	2.04E+03	5.24E+02	3.89E+02
42	TY CrA	8.11E+00	2.32E+01	...	1.24E+00
43	R CrA	1.32E+02	1.53E+02	4.50E+01	2.91E+01
44	T CrA	9.21E+00	1.09E+01	...	4.49E+00
45	BD +404124	3.99E+02	1.57E+03	...	2.89E+01
46	BD +413731	1.94E+02	4.77E+02	...	6.50E+01, 1.10E+02
47	AS 442	9.47E+01	2.11E+02	...	1.38E+01, 3.18E+01
48	LkHα 134	8.60E+01	2.25E+02	...	2.04E+01
49	HD 200775	5.51E+02	1.86E+03	...	3.72E+01, 8.80E+01
50	V645 Cyg	1.29E+05	2.33E+05	5.92E+04	1.75E+04
51	BD +651637	9.95E+01	3.99E+02	...	1.35E+01, 3.19E+01
52	LkHα 234	2.83E+02	5.50E+02	...	1.24E+02
53	BD +463471	1.99E+02	5.08E+02	1.33E+01	4.63E+00
54	LkHα 233	1.01E+02	1.56E+02	...	4.26E+01
55	HD 216629	1.59E+02	1.72E+03	6.87E+00	5.16E+00
57	MWC 1080	7.92E+03	3.03E+04	1.50E+03	1.64E+03

[a] List number given by Finkenzeller & Mundt 1984.
[b] Total luminosity.
[c] Total luminosity corrected for the extinction.
[d] *IRAS* (12–100 μm) contribution. L_{IRAS} is computed when at least the flux at two wavelengths is available.
[e] Correction term L_{corr}. When the last observed flux is affected by extinction, two values of L_{corr}, appropriate to L_{min} and L_{max} respectively, are reported.

μm, some relevant contribution can be expected only for objects whose spectral energy distribution has a significant tail or is still increasing longward of 100 μm. Taking into account the few objects detected at these wavelengths (Harvey et al. 1979; Withcomb et al. 1981; Cohen, Harvey, & Schwartz 1985; Evans, Levreault, & Harvey 1986; Wilking, Mundy, & Schwartz 1986; Beckwith et al. 1990), we computed contributions to the luminosity longward of 100 μm always comparable with the luminosity correction L_{corr}.

To evaluate the relative influence of the *IRAS* data on the luminosities considered to this point to locate these objects in the H-R diagram (Strom et al. 1972; Finkenzeller & Mundt 1984), in Figure 4 we present a histogram of the ratio between the far-IR (L_{IRAS}) and the visual/near-IR (L^{U-Q}) contribution each one with the corresponding correction. If we consider L^{U-Q}_{min} values (Fig. 4, *solid line*), then for nine objects the far-IR contribution to the total luminosity exceeds the optical/near-IR one. This number falls to only two objects if we consider

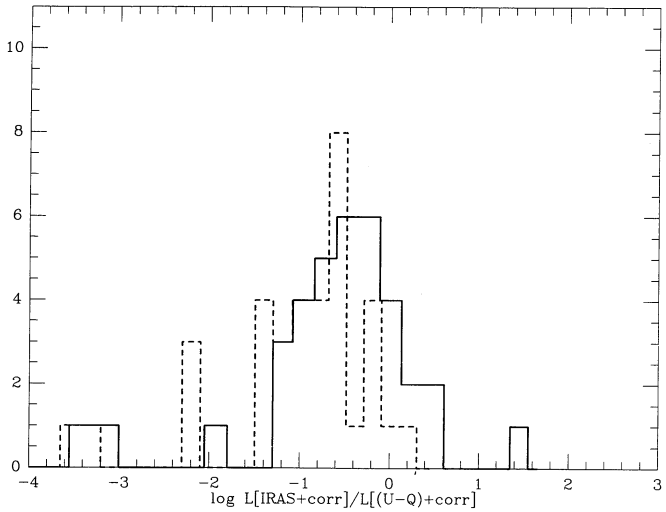

FIG. 4.—The distributions of the far-IR to optical/near-IR luminosity ratio, obtained with L_{min}^{U-Q} (*solid line*) and L_{max}^{U-Q} (*dashed line*).

L_{max}^{U-Q} values (Fig. 4, *dashed line*) corresponding to an extinction assumed of interstellar origin. This suggests that, for more than the 80% of the sources the position in the H-R diagram will be slightly modified, but to a lesser extent than it could result from a 10% uncertainty in the distance estimate.

In Figures 5*a* and 5*b* the H-R diagram for these stars is presented, based on the spectral types listed in the Appendix (Table 8) and converted into effective temperatures adopting the scale given by Cohen & Kuhi (1979). The right-hand (Fig. 5*a*) and left-hand (Fig. 5*b*) panels refer to L_{max} and L_{min}, respectively, while the uncertainty in spectral type can be estimated from Table 8. The very unlikely position of few stars (which are labeled with their numbers) under the ZAMS line reflects the uncertainty in defining their spectral types, as can be seen when comparing the values given by various authors (Finkenzeller 1985). Such spectral misclassifications can arise by ascribing a photospheric origin to lines which are likely affected by phenomena occurring elsewhere (Catala 1989).

The only object showing an anomalous position in the H-R diagram is Z CMa (number 22 in the upper right-hand corner of Figs 5*a* and 5*b*) which has been recently suggested to be a FU Ori type star on spectroscopic grounds (Hartmann et al.

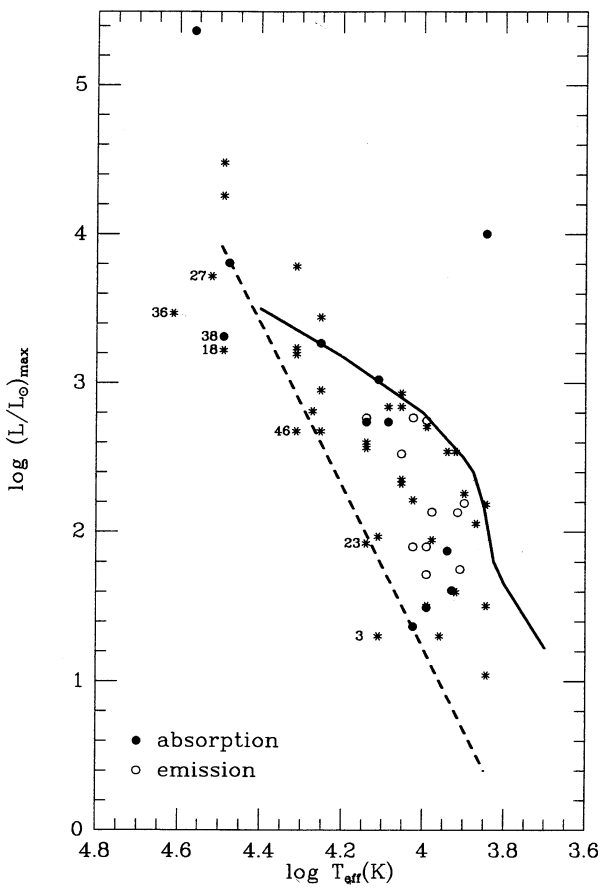

FIG. 5*a*

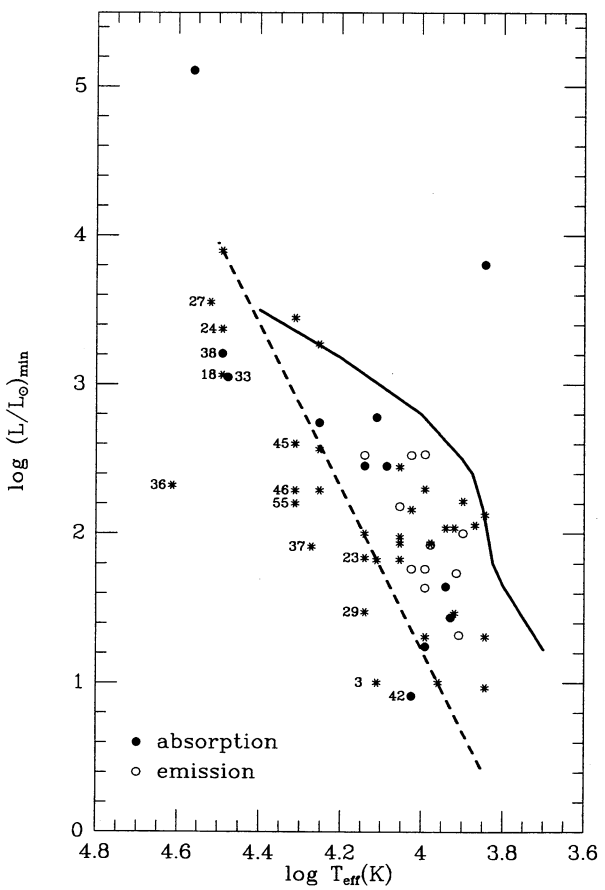

FIG. 5*b*

FIG. 5.—(*a*) H-R diagram for the Herbig Ae/Be stars. L_{max}^{U-Q} (see text) is considered as visual/near-IR contribution to the bolometric luminosity. The straight line identifies the ZAMs, while the curve indicates the theoretical birthline for high-mass stars. Horizontal bars connect positions corresponding to different spectral types attributed to the same star. The open and dotted circles respectively represent the stars showing a silicate emission or absorption at 9.7 μm, while an asterisk indicates a blackbody behavior at the same wavelength. (*b*) The same as (*a*) except L_{min}^{U-Q} contributions to the bolometric luminosity are considered.

1989; Hessman et al. 1991) and to possess a large optical outflow (Poetzel et al. 1989). If this is the case, the observed luminosity could include contributions arising from dissipational processes, e.g., within a disk structure, that are not directly related to the starlight. An alternative explanation of the high luminosity is provided by Koresko, Beckwith, & Sargent (1989) who suggest the presence of a nearby cool and luminous companion in the initial stages of the accretion, which could give a significant contribution to the bolometric luminosity.

In both panels of Figure 5, the continuous curve corresponds to the birthline computed by Palla & Stahler (1990) for stars of intermediate mass ($2 < M_*/M_\odot < 10$). These authors pointed out the agreement between their theoretical birthline and the distribution of 22 Herbig Ae/Be stars listed by Finkenzeller & Mundt (1984). Here the correlation between the H-R diagram of the Herbig Ae/Be stars and the theoretical birth line appears strengthened by the wider and more complete sample (52 of the 57 objects of the Finkenzeller & Mundt 1984 list) and by the consideration of the far-IR contributions to the luminosities. Considering the L_{max} plot (Fig. 5*a*) a slight deviation from the behavior predicted by the theoretical birth line apparently occurs at stellar masses higher than 5 $M_\odot$. By comparing the two diagrams (Figs. 5*a* and 5*b*), we see this deviation is strongly related to the assumed extinction. If we suppose a predominant CS contribution, the suggestion that no optically visible pre–main-sequence phase has to be expected for high-mass stars (Palla & Stahler 1990) is supported. As far as the occurrence of the silicate feature is concerned we note that (see Fig. 5*a*) while the objects showing this feature in absorption are spread over the diagram, those with an emission feature are confined in an area whose center is located at $\log L_{max} = 2.20$, $\log L_{min} = 1.95$ and $\log T = 3.978$ (corresponding to a spectral type A1) with a small dispersion ($\Delta \log L_{max} = 0.44$, $\Delta \log L_{min} = 0.38$ and spectral types B9–A6). If we suppose that the silicate feature is observed in emission or in absorption depending on the inclination of the CS dust disk (Cohen & Witteborn 1985), it is difficult to explain why only stars lying in a defined locus in the H-R diagram are seen in pole-on orientation. Perhaps evolutionary effects rather than the inclination of the CS disks play a dominant role in determining this behavior.

5. THE CONTINUUM SPECTRUM

In this section we describe the model used for computing synthetic spectra to be compared with the observed ones. The starting point is that the stars we are dealing with are observed to be associated with an ambient medium of dust and gas. Besides the hydrogen ionization region and the dust shell, the model considers the presence of a low-ionization Z II region in which metals with ionization potential lower than the Lyman limit are photoionized.

5.1. *The Model*

5.1.1. *Geometry*

Figure 6 shows the adopted disk geometry characterized by its opening angle θ, along with a typical structure of the ionization and dust regions. The spherical case is recovered in the limit of $\theta = \pi/2$. For the sake of simplicity, we assume a pole-on view, the effect of the line-of-sight inclination being easily evaluable in the two extreme cases of optically thin and thick disks.

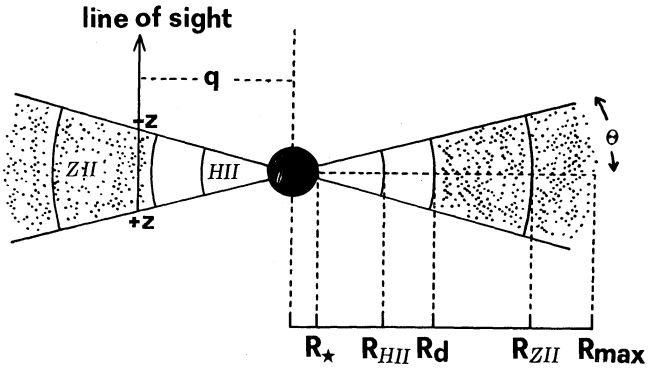

FIG. 6.—Schematic model of the geometry adopted in computing the spectra.

5.1.2. *Radiation Transfer*

Following the usual scheme (see, e.g., Lamers & Waters 1984) the expected flux F_ν, in units of the stellar flux F_ν^*, is derived by solving the radiation transfer equation. In integral form, we define a monochromatic flux ratio as

$$Z_\nu = \frac{F_\nu}{F_\nu^*} = \int_0^{R_{max}} 2q \frac{I_\nu(q)}{I_\nu^2}\, dq\,, \tag{3}$$

where q is the impact parameter at the line of sight, $I_\nu(q)$ is the corresponding emerging intensity

$$I_\nu(q) = \int_{-z_{max}}^{+z_{max}} j_\nu(z) e^{-\tau_\nu(z)}\, dz\,, \tag{4}$$

and $\tau_\nu(z)$ is the optical depth

$$\tau_\nu(z) = \int_z^{-z_{max}} k_\nu(z')dz'\,. \tag{5}$$

The total opacity k_ν and the emission coefficient j_ν are derived as a sum of contributions due to the radiative properties of both gas and dust.

These equations are solved in a disk geometry (Fig. 6), taking into account that dust and gas coexist and that, as early suggested by Dyck & Milkey (1972), the presence of the Z II region has relevant effects in determining the emission spectrum of the Herbig Ae/Be stars.

5.1.3. *Radiative Processes*

The continuum spectrum is emitted as a combination of the dust and gas emission processes which are active, with different efficiencies, in the CS region. In the photoionized H II region, the continuum is emitted through ionic free-free and free-bound radiative transitions, while in the adjacent Z II region the dominant radiative process is free-free between neutrals and electrons. These are provided by the photoionization of metals, mainly carbon, that gives rise to a low electron density. The region of the dust emission is delimited by the dust sublimation temperature and eventually overlaps the H II and/or the Z II region.

We have, considered four major radiative processes: free-free, free-bound, electron scattering, and, finally, dust emission.

The absorption coefficient for ionic free-free and free-bound processes is given by (Brusaard & Van de Hulst 1962)

$$k_\nu^{ff+fb} = \frac{4}{3}\sqrt{\pi}\frac{Z^2e^6}{hcm^{3/2}}\left(\frac{3}{2}kT\right)^{-1/2} \times \nu^{-3} n_e n_i (1 - e^{-h\nu/kT})[g_\nu(T) + b_\nu(T)] \tag{6}$$

while for the case of electron-atom free-free processes we have (Gould 1985, 1986)

$$k_\nu^{\text{e-atom}} = \frac{\sqrt{2}}{3\pi^{5/2}}\,\alpha\sigma_e\left(\frac{kT}{m}\right)^{3/2}\nu^{-3}n_e\,n_a(e^{-h\nu/kT}-1)I_\nu(T) \quad (7)$$

and, finally, for the electron scattering (Allen 1973)

$$k_\nu^{\text{sca}} = 0.66524\times 10^{-24}\left(1-\frac{2h\nu}{mc^2}\right)n_e\,. \quad (8)$$

Here n_e, n_i, and n_a are number densities, for electrons, ions, and atoms, respectively; T is the local gas temperature; α is the fine-structure constant; σ_e is the electron scattering cross section; and $g_\nu(T)$ and $b_\nu(T)$ are free-free and free-bound Gaunt factors. The other symbols retain their usual meanings.

The dust contribution to the total opacity is given by

$$k_\nu^d = \frac{3}{4}\,\frac{Q_\nu(a)}{a}\,\frac{\mu m_{\text{H}}}{\rho_{\text{bulk}}}\left(\frac{D}{G}\right)n_d \quad (9)$$

where the dust absorption efficiency factors $Q_\nu(a)$ are taken from Draine & Lee (1984), a is the dust grain radius, (D/G) is the dust-to-gas mass ratio, ρ_{bulk} is the bulk mass density, and n_d is the grains number density.

In our application the absorption coefficients k_ν are computed as function of the radial coordinate r once the density and temperature are given. An index α characterizes, in this model, the density profile given by

$$\rho(r) = \rho_0\left(\frac{r_0}{r}\right)^\alpha . \quad (10)$$

Equation (10) allows us to obtain the relevant number densities entering the absorption coefficients, once the molecular weight, the ionization degree and the dust-to-gas mass ratio are given. In particular, we assume a constant dust to gas ratio, complete ionization in the H II region and the presence of neutral hydrogen and ionized carbon in the Z II region.

Moreover, a limitation is imposed to the presence of dust by its sublimation temperature, which prevents the dust grain survival up to a critical distance R_{dust} from the star.

The determination of the gas temperature in the envelope is a more difficult task, particularly in the Z II region, because it involves consideration of chemical reaction chains, that, in turn, depend on the radiation field and the gas temperature (see, e.g., Tielens & Hollenbach 1985). In the following we adopt $T_{\text{H II}} = 10^4$ K and $T_{Z\text{ II}} = 3\times 10^3$ K, which are reasonable estimates of the average equilibrium temperatures in an H II region and in the circumstellar Z II region (Dyck & Milkey 1972). Clearly the temperature gradient that results at the interface between the H II and Z II regions is somewhat artificial, and a self-consistent approach should take into account the mutual interaction of temperature and density. However, we expect that the transition region is a negligible fraction of the total emitting volume so that our results on the continuum spectrum should not depend on the exact modeling of the interfaces.

5.1.4. *Dimensions*

The dimensions $R_{\text{H II}}$ and $R_{Z\text{ II}}$ of the corresponding ionized regions have been computed by requiring statistical balance between the production rate of stellar ionizing photons and the recombination rate of hydrogen and metals. We always obtain finite values for $R_{\text{H II}}$ and $R_{Z\text{ II}}$ (ionization-bounded cases) as a consequence of assuming a background gas density. In effect, the location of young stars in the neighborhood of large interstellar clouds suggests that the density in the CS envelope does not decrease indefinitely with distance, but rather tends to a limiting value given by the ambient cloud density.

5.1.5. *Model Parameters*

According to the previous computational scheme, the results of the model depend on a set of physical parameters. However, because here we are interested in the Herbig Ae/Be stars, at least some parameters are guessed on the basis of the nature of these objects. In fact the values of the stellar temperatures T_* for pre–main-sequence stars have been taken from Cohen & Kuhi (1979; see Table 8), while the radii R_* have been taken according to the main-sequence values corresponding to the relevant spectral types.

The extent of the dust region is considered according to a grain sublimation temperature of 1500 K, and the dust-to-gas mass ratio (D/G) has been taken as 0.01, as generally derived in the interstellar medium and in CS envelopes.

The last parameter we have adopted is the ambient density of the parent molecular cloud which has been set to a value of $10\ \text{cm}^{-3}$

5.2. *Numerical Results and Comparison with the Observations*

In Figure 7 we show, for spectral types B0, B5, and A0, typical excesses as defined in equation (3) and obtained for selected values of the model parameters. Though an extensive review of the computed models will be given elsewhere, here it is worth summarizing the general trends observed in the spectra with respect to the variation of the most important parameters.

ρ_0.—The main effect of increasing the initial density ρ_0 is the shrinking of the ionized regions. Consequently the spectrum becomes dominated by the dust emission and the radio excess decreases in favor of a more pronounced excess at 100 μm.

θ.—The aperture of the disk influences mainly the visibility of the star and thus the spectral shape at the shorter wavelengths. For low values of θ (physically thin disks), the excess is greatly reduced in the short-wavelength region so that these models are clearly recognized on the right-hand side of Figure 7.

α.—The variation of the density law index affects the size of the ionized regions and involves optical depth effects. The consequences on the computed excess due to the assumption of constant density ($\alpha = 0$) are shown in the upper left-hand panel of Figure 7.

To allow a comparison with the observed spectral shapes, in Figure 8 we present the excesses as derived from the observations of these Herbig Ae/Be stars detected up to the radio wavelengths (Altenhoff et al. 1976; Cohen, Bieging, & Schwartz 1982; Bieging, Cohen, & Schwartz 1984; Güdel et al. 1989; Curiel et al. 1989; Skinner, Brown, & Linsky 1990). The excesses are derived, taking into account that

$$Z_\nu = \frac{F_\nu}{F_V}\,\frac{F_V^*}{F_\nu^*}\,\frac{F_V}{F_V^*}\,, \quad (11)$$

where the meaning of the symbols is the same as in equation (3) and the subscript V denotes the visual band. The first term on the right-hand side of this expression is computed from the observed fluxes, the second is derived from the photospheric emission of the given spectral type, and the last one depends on the visual absorption.

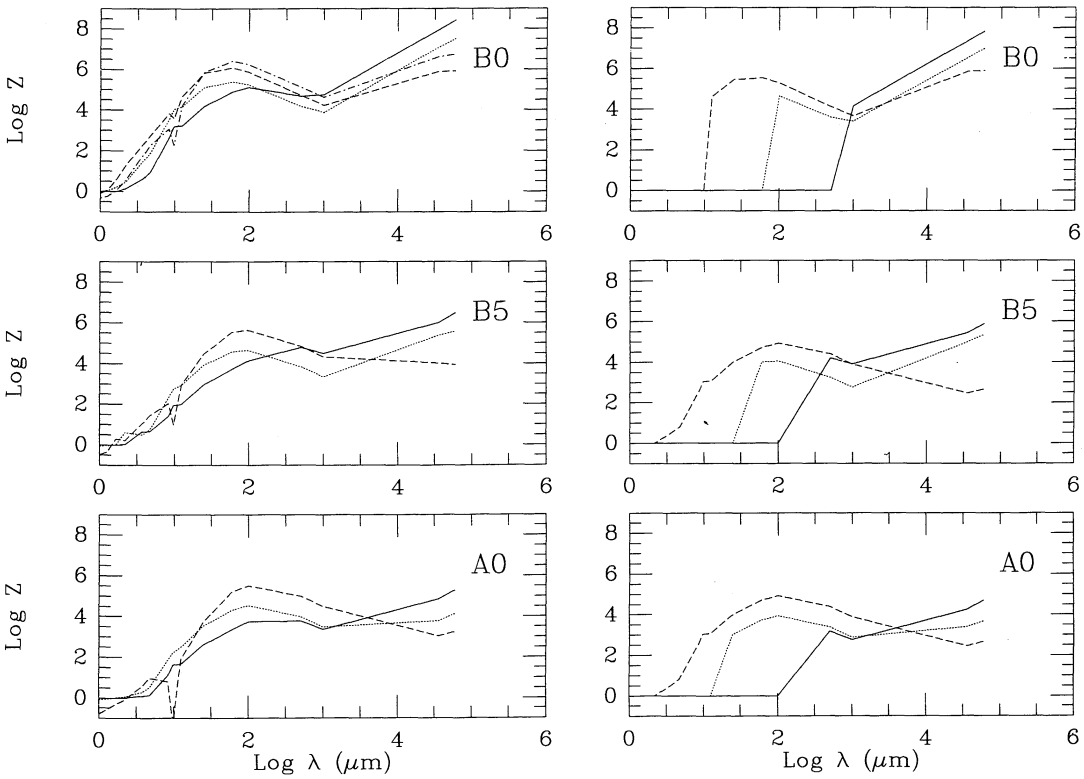

FIG. 7.—Computational results. For spectral types B0, B5, and A0 the excess Z (see text, eq. [3]) is shown as a function of the wavelength for a density profile $\rho(r) \propto r^{-0.5}$ and selected values of the initial density. Left and right panels refer, respectively, to cases with $\theta = 90°$ (spherical envelope) and $\theta = 15°$ (disk). In the upper left panel the dash-dotted line shows how the solid line is modified when a constant density is assumed in the corresponding model. Solid, dotted, and dashed lines refer to initial density values of 5×10^6, 5×10^7, and 5×10^8 cm^{-3}, respectively.

If we attempt to fit the observations with the computed models we note the following:

1. The slope of the excess between 1 and 100 μm cannot be reconciled with dust-dominated envelopes. This shape is indeed better fitted by models in which the gas processes contribute significantly to the emission. This result confirms, by means of a more accurate radiation transfer model, what has already been pointed out by Dyck & Milkey (1972) and Lorenzetti, Saraceno, & Strafella (1983).

2. All the stars detected in the radio continuum show a prominent excess at these wavelengths with a positive slope (Fig. 8), again indicating that simple dust models are not suited to account for the global spectrum. In fact the radio spectrum is emitted mainly in the ionized regions, and its intensity and slope are sensitive to the details of the density profile in these regions.

3. If we fit the near-IR and radio spectrum, it is found that the *IRAS* fluxes are greater than expected by the models. This fact can be understood taking into account that the observations are affected by a beam size effect, increasing with wavelength, as previously discussed.

It is noticeable that in Figure 8, a better agreement between observations and model is obtained in the spherically symmetric case ($\theta = 90°$) due to the lack of near-IR excess when flattened structures are considered, as shown in Figure 7 ($\theta = 15°$). This model result is due to the dominance of the unobscured stellar photosphere at short wavelengths when the star is directly viewed from the observer. Of course, to obtain a near-IR excess with a disk geometry, we could run models by tuning the initial density at higher values, but this invariably results in a bad matching of the long wavelength excess.

The computed models in Figure 8, to which the observations are fitted, are representative of a density law with $\alpha = 0.5$ and an initial number density $n_0 = 2$–5×10^8 cm^{-3} with the exception of TY CrA and AB Aur for which $n_0 = 5 \times 10^5$ cm^{-3} and $n_0 = 10^9$ cm^{-3}, respectively, have been used. The total mass involved, ranging between 0.006 and 0.6 $M_\odot$, is contained in 4×10^3–10^4 AU that, when spherically distributed, is well compatible with the observed visual extinctions. In these models the dust temperature profile follows a law similar to equation (10) with an exponent 0.5–0.7 and an initial temperature $T_0 = 1500$ K.

Finally, we must mention that models including a circumstellar disk can be quite successful in fitting the same spectral shapes (see, e.g., Adams, Lada, & Shu 1987; Kenyon & Hartmann 1987; Beckwith et al. 1990; Natta et al. 1992). In particular in these models the presence of a disk is required to account for the observed near-IR excess. In this respect the present model shows that, if the free-free emission from a weakly ionized circumstellar region (Z II region) is taken into account, the near-IR spectrum can be naturally fitted as well, without necessarily invoking a disk (see also Dyck & Milkey 1972 and Lorenzetti et al. 1983).

6. DISCUSSION

The extent and homogeneity of the data collected in this work on the Herbig Ae/Be stars allows us to discuss the geometry of the CS envelope in a more statistically significant way than what has been done up to now.

The occurrence or absence of disks is in fact of special interest in the context of the PMS evolution because, for the lower mass T Tauri stars, there are increasing evidences in favor of

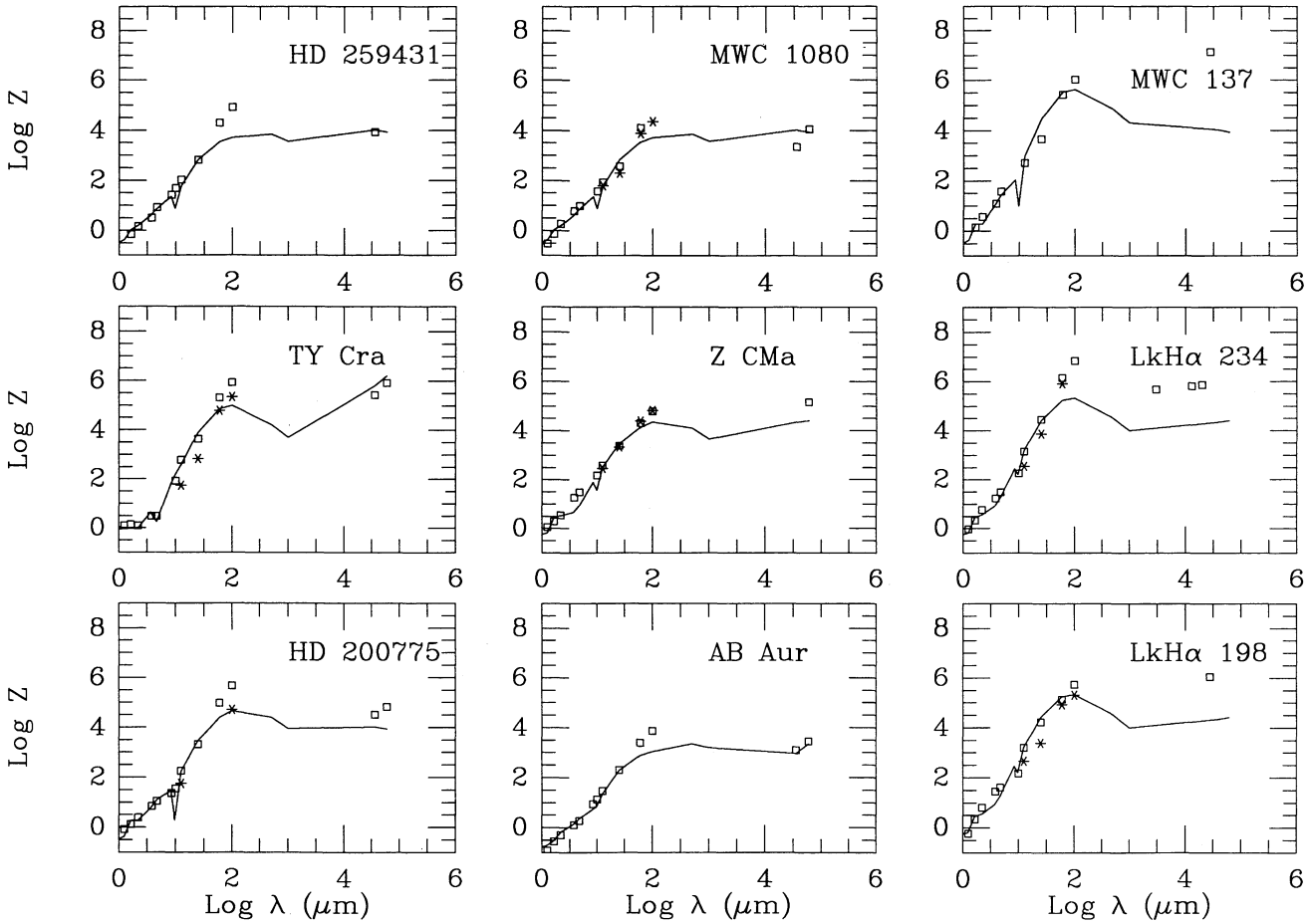

FIG. 8.—Observed excesses. For stars detected up to the radio wavelengths, the observations are compared with the model results. The excesses are derived from the observed fluxes as described in the text. In addition, when available, KAO observations taken from the literature have been reported with starred symbols.

flattened geometries, giving observational grounds to the conjecture that a disk phase occurs during the pre–main-sequence evolution of low-mass stars (see, e.g., Bertout 1989).

6.1. *Two-Color Diagrams*

The near-IR photometry (H, K, L) listed in the Appendix (Table 7) is graphically presented in Figure 9 as a two-color diagram. In the same diagram drawn for a sample of T Tauri stars, Cohen & Witteborn (1985) found a well-defined separation between the stars with silicate emission and those with silicate absorption. This fact was interpreted as a clue of nonspherical geometry in the CS shells of the T Tauri stars. Larger near-IR color indices are in fact expected for edge-on dust disks traced by the 9.7 μm absorption feature, while disks more and more inclined show their inner and warmer parts, reducing the near-IR indices and increasing the occurrence of silicate emission. This interpretation is further supported by the relatively small number of absorption cases (29%) with respect to emission cases (64%) as expected for randomly oriented disks.

If we make a similar comparison for the Herbig Ae/Be stars, the relative number of observed features in absorption (35% of cases against only 32% in emission) prevents a similar conclusion for this class of objects. Moreover, in the two-color diagram of Figure 9, Herbig Ae/Be stars offer no evidence of separation between emission and absorption, suggesting in a pure observational way either different dust geometries or different interpretations of the near-IR excesses (e.g., Lorenzetti et al. 1983). On the contrary, an evident separation is found in Figure 10, where the difference of magnitudes at 12 and 60 μm

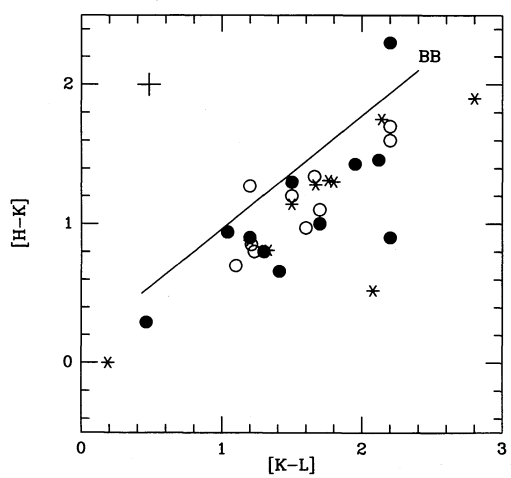

FIG. 9.—Dereddened $[H-K]$, $[K-L]$ color plot for the Herbig Ae/Be stars. The objects exhibiting silicate emission or absorption are indicated with open and filled circles, respectively. Asterisks correspond to objects with a blackbody behavior (flat spectrum) at 9.7 μm. The solid line represents the blackbody temperature scale. The cross in the upper left corner shows the color errors.

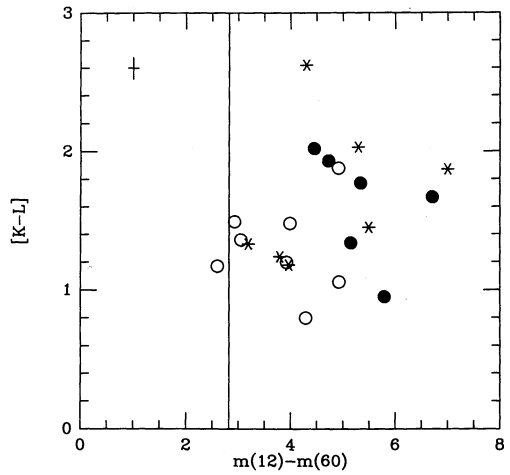

FIG. 10.—Dereddened near-IR color $[K-L]$ vs. *IRAS* $[m(12)-m(60)]$ color (defined in the text). Symbols as in Fig. 9. The vertical line corresponds to a $L^{-4/3}$ slope in the *IRAS* color.

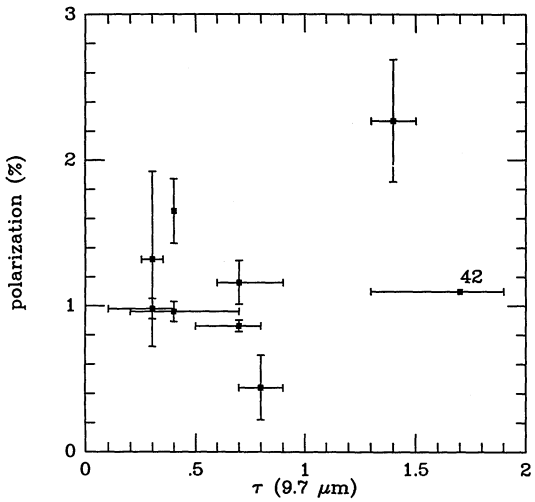

FIG. 11.—Polarization (in percent) measured in the V band (the only exception is the B band value given for object 42) vs. optical depth of the stars showing silicate absorption feature. Vertical bars indicate the range of variability for the polarization (see text), while the horizontal ones refer to the uncertainty in evaluating our $\tau_{9.7\ \mu m}$ (see Fig. 1).

is reported versus the color $[K-L]$ for the stars listed in Tables 2 and 3. The magnitudes at the *IRAS* effective wavelengths have been obtained by converting the values reported in Table 4 with the zero-magnitude corresponding fluxes F_ν[0.0 mag] 28.3 and 1.19 Jy at 12 and 60 μm respectively (Beichman et al. 1985). The objects showing a silicate absorption feature have definitely steeper far-IR spectra with respect to stars with emission feature, while this separation does not appear in the near-IR color index $[K-L]$. Such behavior suggests that the near-infrared spectrum could be related to mechanisms other than dust emission, which is more effectively traced by the longer wavelength emission. The more pronounced steepness we observe in the absorption objects is undoubtedly related to the relative importance of the cold dust in the far-infrared, even if, due to the unfavorable statistics of the absorption cases, it seems more explicable in terms of radiation transfer in a dust envelope than as a consequence of the progressive inclination of a disk.

6.2. *Polarization*

If the CS dust were organized in a flattened geometry, we could expect a positive correlation between the observed polarization and the inclination of the disk to the line of sight. The highest polarization values are expected when the disk prevents the direct view of the starlight and only scattered light is allowed to reach the observer. If this is the case a positive correlation between the optical polarization (P_V) and the dust optical depth of the silicate absorption feature ($\tau_{9.7\ \mu m}$ abs) provides an indication in favor of dusty disks, as shown for the T Tauri stars by Cohen & Witteborn (1985). For the Herbig Ae/Be stars with silicate absorption (Tables 2 and 3) we searched the literature for polarization observations in the visual band, providing in Table 6 the smallest and largest P_V among the observed values given in the references indicated. The individual stars are easily recognized in Figure 11 by means of the vertical bars which account for the maximum range of polarization variability.

One could argue for a correlation if the object N42 (TY CrA) were omitted. In this respect Herbig & Bell (1988) note it is an eclipsing variable, so that in principle polarization and τ_{abs}(9.7 μm) could be related to different objects. However, considering the polarization map of V645 Cyg obtained at about 1 μm by Lenzen (1987), we have for this object $P_{1\ \mu m} \geq 12\%$ (see Table 6), but in Figure 11 the corresponding point at $\tau_{abs}(9.7\ \mu m) = 1.1$ (see Table 3) is omitted due to the different wavelength of observation. In any case, because the differences in polarization measured so far between the I and V bands very rarely exceed a factor of 2, we may adopt for V645 Cyg a conservative value of $P_V \sim 6\%$, showing that a correlation in Figure 11 is at least questionable.

The absence of any clear correlation suggests again that a disk geometry for the CS dust distribution hardly could be appropriate to Herbig Ae/Be stars.

TABLE 6

OPTICAL POLARIZATION OF HERBIG Ae/Be STARS SHOWING SILICATE ABSORPTION

Number[a]	Source	P_V	Reference
6	HK Ori	1.01%–1.31%	1, 2, 3
8	T Ori	0.11 –0.55	1, 2, 3, 4
17	HD 259431	0.91 –1.05	1, 2, 4, 5
22	Z CMa[b]	0.82 –0.90 (0.14)	1, 4, 5, (2)
30	HD 97048	1.84 –2.69	6, 7
33	CoD −4211721[c]	...	...
38	MWC 297	1.43 –1.87	3
42	TY CrA	1.1 (B band)	8
49	HD 200775	0.89 –1.02	1, 3, 5, 9
50	V645 Cyg[d]	12 (1 μm)	10
52	LkHα 234	0.72 –1.91	2, 3, 9

NOTE.—Range of the observed polarization in the V band (unless otherwise indicated) are given for each star showing a silicate absorption at 9.7 μm.

[a] List number given by Finkenzeller & Mundt 1984.

[b] The minimum value (indicated in parentheses) was quite unusual with respect to other determinations, and it is not considered in Fig. 11.

[c] No determination of the visual polarization is available in the literature.

[d] The polarization is detected at 1 μm therefore, it was not considered in Fig. 11, although it reinforces the absence of any correlation (see text).

REFERENCES.—(1) Breger 1974. (2) Garrison & Anderson 1978. (3) Vrba, Schmidt, & Hintzen 1979. (4) Jain, Bhatt, & Sagar 1990. (5) Vrba 1975. (6) Bastien 1985. (7) Drissen, Bastien, & St. Louis 1989. (8) Serkowsky 1969. (9) Petrova & Shevchenko 1987. (10) Lenzen 1987.

6.3. *Far-IR Luminosities*

The lack of a positive correlation between the distance and the visual absorption for the Herbig Ae/Be stars, suggests a prevalently CS origin for the extinction, as evidenced in Table 8 by the many relatively nearby objects with high A_V values. Then, if most of the extinction originates in a spherical CS environment, the absorption toward a source, measured by the parameter A_V, should be related to the intrinsic properties of the envelope itself. One such property is the far-infrared luminosity that is expected to be related to the CS dust content and thus, by searching for correlation with the extinction, can be used to check the hypothesis on the geometry of the dust distribution around the Herbig Ae/Be stars.

We adopted the ratio between the far-IR luminosity ($L_{IRAS} + L_{corr}$) and the optical near-IR one (L_{U-M}) as a measure of the CS dust content. In fact the luminosity ratio seems more suitable to evaluate the dust capability to reprocess the stellar photons than a spectral index α ($\alpha = d \log \lambda F_\lambda / d \log \lambda$, in the 2–60 μm range), the latter being strongly dependent on the choice of the wavelengths and poorly defined when we deal with a complex spectral shape.

The luminosity ratios as a function of the observed visual extinction are shown in Figure 12 where the best linear fit to the observed points (*filled circles*) is indicated giving a correlation coefficient of 0.52, corresponding to a probability close to 100% that the variables are correlated. In the same figure the luminosity ratios obtained with the same spherical models of Figure 7 are shown, for comparison, as open symbols.

This correlation suggests that the global trend is in agreement with a spherical distribution of the CS material responsible for the far-IR luminosities of the Herbig Ae/Be stars. In fact, a disk structure would permit an unobscured view of the central star, and no correlation should be observed, unless the disks are prevalently seen edge-on or possess extreme flaring.

The observational parameters so far considered, consistently give indication of prevailing spherical symmetries in the IR-emitting CS envelopes. However, as pointed out in the Introduction, there are in the literature some observations that were interpreted as indirect evidences of flattened geometries around a dozen of these stars. The obvious question that arises is how can these interpretations be reconciled with the global results presented in this work?

Another check of the disk hypothesis as a common feature of the Herbig Ae/Be stars can be made if we attempt to select disks seen pole-on among our sample. In this respect we can use the fact that, for disks seen pole-on, the stellar photosphere should be unobscured at the shorter wavelengths if the extinction is of circumstellar origin.

Applying this criterion, a search for photospheric spectral shapes in the visual–near-IR (color indices ~ 0; see Table 7) selects four objects (HD 37490, HD 52721, HD 76534, and BD +413731) for which we have no independent disk evidence in the literature. It is possible to envisage two possibilities to understand this discrepancy: either (*a*) the objects found in the literature are edge on cases or (*b*) the disks play a role at a spatial scale smaller than that probed by the adopted selection criterion and they do not actually determine the IR-emitting properties of these stars.

The first case (*a*) is ruled out considering that, if the disks are of similar half-aperture θ and randomly oriented, the probabil-

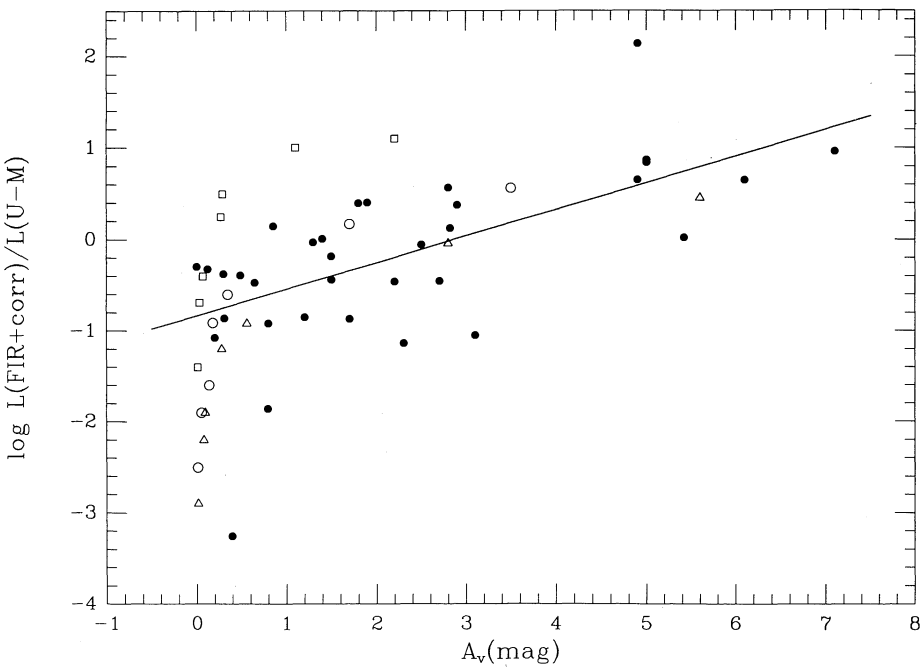

FIG. 12.—Luminosity ratio (see text) vs. visual extinction (A_V) for the Herbig Ae/Be stars. The open symbols represent the location in this diagram of the same spherical models shown in Fig. 7; squares, circles, and triangles refer to the spectral types B0, B5, and A0, respectively.

ity of observing edge-on cases is approximately given by the fraction of the total solid angle subtended by the disk, namely sin θ. In this case the fact we suspect the presence of disks for a dozen of 57 objects implies an opening angle of $\theta \sim 12°$, suggesting in turn that the adopted criterion should be able to pick up many more pole-on cases than the four actually selected.

It appears thus more appropriate that the indirect evidences of disks or flattened geometries previously reported in the literature are a manifestation of processes occurring at smaller spatial scale, not directly related to the infrared-emitting envelope. The spatial extent of this envelope, as computed in the model described above, is in fact of the order of 10^5–$10^6 R_*$ so that its geometry is not necessarily related to the wind-chromosphere complex where optical-UV line profiles are formed and polarization and collimation of mass outflows can occur.

7. CONCLUSIONS

Below, we briefly summarize the main conclusions of this work.

1. Silicate features, both in emission and absorption, are commonly observed for Herbig Ae/Be stars in the 10 μm spectral region. The physical parameters, as the optical depth at 9.7 μm ($\tau_{9.7}$ μm) and the dust temperature ($T_{\rm dust}$), derived from the three filter photometry ($N1$, $N2$, $N3$), are in good agreement with the values obtained from more resolved spectral energy distributions (CVF spectra).

2. The presence of dust around these stars is confirmed by their high association rate (70%) with an *IRAS* counterpart. The distribution of these stars in the *IRAS* two-color diagram appears more scattered with respect to the locus where the T Tauri stars cluster. A significant dispersion exists with respect to the color corresponding to an accretion or reprocessing disk.

3. Composite energy distributions for these stars up to 100 μm show that for more than 80% of the sources, the position on the H-R diagram is only marginally affected by including the *IRAS* fluxes.

4. Correlations among the parameters, either derived in this work (near-IR colrs, [$\tau_{\rm abs}$(9.7 μm)], far-IR luminosities) or available in the literature (visual polarization and extinction), give support to a spherical geometry for the dust distribution.

5. An emission model, taking into account radiative properties both of gas and dust, provides a satisfactory agreement with the observations up to the radio wavelengths, without requiring a disk geometry. The near-IR excess in this model is produced by a low-ionization region in which metals with ionization potential less than 13.6 eV are photoionized.

6. On the contrary there are in the literature some observations that have been interpreted as evidence of flattened geometries around a dozen of these stars. These interpretations could be reconciled with the global results presented here if those evidences are manifestations of processes occurring at a smaller spatial scale (hundreds of AU) with respect to that typical of the far-infrared–emitting envelope (thousands of AU). In any case, the presence of a circumstellar disk cannot be considered a well-grounded statement for the class of the Herbig Ae/Be stars.

7. The fact that, differently from the T Tauri stars, disk structures seem not to be a global property of the IR-emitting envelope of the Herbig Ae/Be stars has, from an evolutionary point of view, two possible interpretations as a result of either different processes prevailing in the PMS phase of low- and high-mass stars or, merely, different durations of the disk phase.

A final conclusion appears premature because both the observational search for evidence of disks around the Herbig stars is far from being complete and the theoretical background is relatively poorly defined.

The authors thank Francesco Palla for useful discussions on modeling of circumstellar envelopes. Thanks are also due to an anonymous referee for useful comments on this work.

APPENDIX

This appendix reports the data we used to compute the bolometric luminosities and to obtained the H-R diagram for the Herbig Ae/Be stars. In Table 7 multiwavelength photometric data are reported, while in Table 8 complementary information is listed. Complete references are also given to the literature in reference lists to the tables.

TABLE 7

PHOTOMETRY OF THE HERBIG Ae/Be STARS

N.	Source	U	B	V	R	I	Ref. Opt.	J	H	K	L	M	Ref. Near IR	N	Q	Ref. Mid. IR	IRAS
1	LKHα 198	15.50	15.26	14.29	12.93	11.74	20	9.9	7.9	6.3	4.1	3.7	1	1.41	-0.3	2,9	*
2	BD+61154	10.80	11.12	10.61			20	8.5	6.9	5.7	4.2	4.0	1	1.81		2	*
3	XY Per	10.40	9.88	9.36			20		6.81	6.07	5.04	4.3	4,5	2.0		5	*
4	Elias 1		16.8	15.3			20	8.55	6.91	5.64	4.44	3.84	6	0.54	-1.9	6	*
5	AB Aur	7.22	7.21	7.07	6.82	6.68	20	6.1	5.1	4.4	3.3	2.9	1	0.52	-1.6	2,7	*
6	HK Ori	12.13	12.11	11.63	11.21	10.75	20	9.4	8.4	7.4	5.7	4.9	1	2.56	1.0	2,11	*
7	BD+9880	10.05	10.07	9.93			20		8.87	8.26	7.46		48				*
8	T Ori	10.62	10.36	9.96	9.70	9.40	20	8.4	7.4	6.5	5.3	4.8	1	2.86		2	
9	V380 Ori	10.19	10.44	10.00	9.59	9.12	20	8.0	7.0	5.9	4.2	3.7	1	1.89	0.3	2,11	*
10	BF Ori	10.97	10.50	10.32	10.20	9.96	20	9.19	8.55	7.98	6.6		10	3.1		11	*
11	RR Tau	11.70	11.40	10.90			20	9.7	8.3	7.1	5.8	5.5	1	3.1	0.2	11	*
12	HD 37490	3.61	4.42	4.50			23	4.53	4.51	4.51	4.32	4.32	49	3.13		8	*
13	HD 250550	9.24	9.53	9.48	9.39	9.28	20		7.65	6.77	5.57	4.3	4,5	2.72	0.4	2,9	*
14	LKHα 208	13.52	13.21	12.74			20		9.85	8.88	7.28		4	2.3	0.7	5	*
15	MWC 137	12.96	13.23	12.05			20		7.48	6.41	5.07	3.87	4,50	2.18	0.92	50	*
16	LKHα 215	10.96	10.93	10.42	9.99	9.54	20	5.9	5.6	5.5	5.4	5.4	1	4.0	2.1	46	
17	HD 259431	8.43	8.96	8.69	8.38	8.09	20		6.56	5.62	4.58	3.51	4,46	1.39	0.1	2,11	*
18	R Mon	11.72	12.08	11.32	10.54	9.94	20	9.5	7.8	5.9	3.1	1.8	1,11	-0.2	-2.4	11	*
19	LHKα 25	12.95	12.93	12.78	12.34	11.82	20	11.77	10.73	9.42	7.66	6.57	12	3.14	1.22	12	*
20	HD 52721	5.90	6.64	6.58			23	6.29	6.23	6.10	5.96	5.68	13,46				*
21	LKHα 218			12.2			20		9.1	8.5			4				*
22	Z CMa	11.24	10.56	9.35	8.57	7.80	20	5.7	4.7	3.8	1.6	1.0	1	-1.14	-3.2	2,11	*
23	LKHα 220			12.3			20		9.8	8.9			4				*
24	HD 53367	6.82	7.41	6.97			23	5.76	5.48	5.18	4.81	4.46	13,46	2.1		14	*
25	CoD-443318	10.47	10.31	9.84	9.48	9.04	20	8.08	6.96	5.87	4.27	3.85	3				*
26	HD 76534	7.54	8.11	7.96	7.83	7.70	26	7.64	7.58	7.42	7.06		3				*
27	RCW 34	12.61	12.73	11.81			24	9.24	8.84	8.54	7.2		3,14	2.1		14	*
28	RCW 36							8.34	7.19	6.57	6.19	6.20	3				*
29	Herbst 28	12.20	12.00	11.28			24	9.50	9.22	9.07			3				
30	HD 97048	9.00	8.80	8.45	8.19	7.93	20	7.40	6.89	6.22	4.80	4.68	3	2.53		3	*
31	HR 5999	7.30	7.10	6.79	6.59	6.37	20	5.73	5.07	4.25	2.91	2.55	3	0.97		3	*
32	HD 150193							7.02	6.28	5.47	4.23	3.93	3	0.97	-0.4	3,15	*
33	CoD-4211721	12.59	12.71	11.43			20	7.36	5.98	4.51	2.38	1.75	3	0.23		3	*
34	KK Oph	11.43	10.99	10.32			20	8.52	6.99	5.64	3.97	2.59	3	1.37		3	*
35	HD 163296	6.99	6.92	6.85	6.78	6.70	26	6.28	5.58	4.72	3.50	3.18	3	0.69		3	*
36	LKHα 118	11.75	12.04	11.16	10.48	9.80	27	8.88	8.40	7.99	7.54		3				
37	LKHα 119	13.08	12.99	12.16	12.12	10.91	27	9.83	9.40	9.04	8.30		3				
38	MWC 297	15.00	14.17	12.04	9.73	8.08	28	6.35	4.63	3.19	1.23	0.58	3	-1.17	-2.46	3,7	*
39	VV Ser	13.72	13.21	12.14			21	8.77	7.47	6.32	4.81	4.34	3	2.38		3	*
41	AS 310	13.88	13.42	12.49			20	10.34	10.03	9.48	7.39		3	2.45	-0.1	3,9	*
42	TY CrA	9.47	9.39	8.95	8.57	8.14	20	7.56	7.02	6.70	6.23	5.56	3	2.72	0.1	3,43	
43	R CrA	11.40	11.30	10.74	9.72	8.10	20	7.53	5.41	3.63	1.48	0.93	3	-0.97	-3.3	3,43	*
44	T CrA	14.28	14.08	13.37	12.77	12.17	20	9.25	7.75	6.44	4.76	4.31	3	2.35	-1.3	3,43	
45	BD+404124	10.95	11.30	10.52			20	8.0	6.9	5.7	4.2	3.8	1	1.5	0.8	47	
46	BD+413731	9.47	9.97	9.88			20	9.9	9.8	9.9	9.6		1	2.3		17	
47	AS 442	11.84	11.50	10.87			53		7.75	6.46	5.16	4.3	18,16	3.0		16	
48	LKHα 134	12.23	12.03	11.40			53		8.66	7.99	6.79		4	1.7	0.4	16	
49	HD 200775	7.38	7.77	7.39	6.91	6.38	20	6.1	5.5	4.7	3.4	2.9	1	1.59		2	
50	V645 Cyg	15.74	15.16	14.06	12.91		29	9.3	7.1	4.8	2.6	1.2	29	-0.7	-3.0	29	*
51	BD+651637	10.14	10.49	10.08	9.53	9.26	22	9.0	8.7	8.6	8.0	7.5	1	3.8		17	
52	LHKα 234	13.40	13.24	12.35	11.35	10.70	22	9.3	8.1	6.8	5.3	4.7	1	2.43	-0.78	2	
53	BD+463471	10.68	10.50	10.10			20	8.6	7.7	6.7	5.1		1	5.0		17	*
54	LKHα 233	15.24	14.54	13.56	12.62	11.80	30	11.2	10.0	8.3	6.1	5.5	1	2.63	0.1	2,9	
55	HD 216629	9.82	10.01	9.29			23	7.25	6.84	6.36	6.69		3				*
56	BHJ 71	11.75	11.38	10.57				8.44	7.97	7.55	6.99		3				
57	MWC 1080	13.35	13.10	11.67	10.16	8.92	20	7.4	6.0	4.7	2.9	2.4	1	0.82	-0.3	2,9	*

EXPLANATION OF COLUMNS.—Col. (1): Catalog number according to Finkenzeller & Mundt 1984. Col. (2): Star identification. Cols. (3)–(7): *UBVRI* observed magnitudes. Col. (8): References for the optical photometry. Cols. (9)–(13): *JHKLM* observed magnitudes. Col. (14): References for near-IR photometry. Cols. (15) and (16): *N* (10 μm) and *Q* (20 μm) observed magnitudes. Col. (17): References for *N*, *Q* photometry. Col. (18): The presence of an *IRAS* counterpart (see § 3) is indicated by an asterisk (*).

NOTES.—(1) The observations in the IR bands *L*, *M*, *N*, and *Q* are obtained with slightly different filters whose effective wavelengths are quoted in the individual references. (2) The variability (both in the optical and in the IR bands) is quite an usual property of these stars. However, the values listed in this table do not account for this, although we tried (whenever it was possible) to report simultaneous observations in different bands. (3) Upper limits (in any band) have not been considered. (4) In optical and infrared bands, the fluxes have been derived from the magnitudes according to the Johnson (Johnson 1965) and ESO (Bouchet et al. 1989) calibration systems.

REFERENCES.—(1) Lorenzetti, Saraceno, & Strafella 1983; (2) Berrilli et al. 1987; (3) Present work; (4) D. A. Allen 1973; (5) Cohen 1973b; (6) Elias 1978; (7) Simon 1974; (8) Gehrz, Hackwell, & Jones 1974; (9) Cohen 1974; (10) Glass, & Penston 1974; (11) Cohen 1973c; (12) Rydgren, & Vrba 1987; (13) Whittet, & Van Breda 1980; (14) Williams, Beattie, & Stewart 1977; (15) Elias 1978; (16) Cohen 1973a; (17) Strom et al. 1972b; (18) Cohen, & Kuhi 1979; (20) Herbig & Bell 1988; (21) Bastian, & Mundt 1979; (22) Shevchenko & Yakubov 1989; (23) Racine 1968; (24) Herbst 1975; (26) Thè et al. 1985; (27) Boesono, Thè, & Tjin A Djie 1987; (28) Bergner et al. 1988; (29) Humphreys, Merrill, & Black 1980; (30) Chernyshev & Shevchenko 1988; (43) Knacke et al. 1973; (46) Herbst et al. 1982; (47) Cohen 1972; (48) Penston, Allen, & Lloyd 1976; (49) Dachs, & Wamsteker 1982; (50) Cohen & Barlow 1975; (53) Petrova, & Shevchenko 1987.

TABLE 8

SPECTRAL TYPES, EXTINCTIONS, AND DISTANCES FOR HERBIG Ae/Be STARS

N.	Sp.T.	Ref.	T_{eff} (K)	Ref.	A_V(mag)	Ref.	D(pc)	Ref.	N.	Sp.T.	Ref.	T_{eff} (K)	Ref.	A_V(mag)	Ref.	D(pc)	Ref.
1	A	51	9800	18	5.0	37	600	37	29	B5	14	13800	18	3.1	14	870	34
2	B8	31	11300	18	2.2	31	650	31	30	A0	31	9800	18	1.3	31	150	39
3	A2/B6	31	12900/9100	18	1.2	23	160	38	31	A7	31	7900	18	0.2	31	270	31
4	A6	18	8100	18	6.10	18	140	6	32	A0	31	9800	18				
5	B9-A0	18	10600/9800	18	0.65	18	160	31	33	B0	35	30000	35	7.1	35	400	35
6	A4	31	8500	18	1.5	31	460	31	34	A5	35	8200	35	2.7	35	310	35
7	A5	32	8300	18	0.49	32	400	32	35	A0	26	9800	18	0.31	26	150	26
8	A3	31	8700	18	1.1	31	460	31	36	O6	27	41000	27	3.7	27	1900	27
9	A1	31	9500	18	1.5	31	460	31	37	B3	27	18700	27	3.2	27	1900	27
10	A/F	31	9800/7000	18	0.8	31	460	38	38	B0	28	30900	18	2.9	36	450	36
11	A3/A5	31	8700/8300	18	2.5	31	800	31	39	B1/B3	31	22600/17900	18	4.2	31	245	44
12	B3	31	17900	18	0.4	31	360	23	41	B0	18	30900	18	3.34	18		
13	B9	31	10600	18	0.3	31	700	31	42	B9	31	10600	18	1.7	31	150	43
14	B5/B9	31	13800/10600	18	1.8	31	2000	31	43	F0	31	7000	18	1.9	31	150	31
15							900	50	44	F0	31	7000	18	1.7	31	150	31
16	B7/B8	31	12200/11300	18	2.5	31	800	31	45	B2	31	20500	18	3.0	31	1000	31
17	B6	31	12900	18	1.4	31	800	31	46	B2/B3	31	20500/17900	18	1.1	31	1100	31
18	B0	18	30900	18	2.8	31	800	31	47	B8	31	11300	18	1.74	18	700	18
19	B8	31	11300	18	5.0	54	800	31	48	B8	31	11300	18	2.06	18	700	18
20	B2	31	20500	18	0.8	31	1150	31	49	B3	31	17900	18	1.8	31	600	31
21	B6	18	12900	18	1.12	18	1150	46	50	O7	31	36500	52	4.9	41	6000	41
22	F	18	7000	18	2.82	18	1150	31	51	B5	31	13800	18	1.8	31	1000	31
23	B5	18	13800	18	0.86	18	1150	46	52	B5/B7	31	13800/12200	18	3.1	31	1000	31
24	B0	31	30900	18	2.3	31	1150	31	53	A0	31	9800	18	1.7	31	1000	31
25	A1	51	9500	18	0.12	33	450	33	54	A7	31	7900	18	2.2	31	880	31
26	B3	31	17900	18	1.0	31	870	34	55	B2	31	20500	18	3.1	31	725	42
27	O9	14	33000	18	4.9	14	870	34	56	B0/B8	31	30900/11300	18	3.1	31		
28			7400	45			600	45	57	B0	18	30900	18	5.42	18	2500	36

EXPLANATION OF COLUMNS.—Col. (1): Catalog number. Col. (2): Spectral type. Col. (4): Effective temperature of the star. Col. (6): Visual extinction. Col. (8): Adopted distance.

NOTES.—(1) The object XY Per (number 3) is a binary system whose components have the indicated spectral types. (2) R Mon (number 18) has a very uncertain spectral classification. In the literature the assigned spectral type ranges from B to K. (3) For the star VV Ser (number 39) the distance of the cloud is adopted, which gives a lower limit to the luminosity.

REFERENCES.—(6) Elias 1978; (14) Williams, Beattie, & Stewart 1977; (18) Cohen & Kuhi 1979; (23) Racine 1968; (26) Thè et al. 1985; (27) Boesono, Thè, & Tjin A Djie 1987; (28) Bergner et al. 1988; (31) Finkenzeller & Mundt 1984; (32) Murdin & Penston 1977); (33) Brandt et al. 1971; (34) Herbst 1975; (35) De Winter & Thè 1990; (36) Cantò et al. 1984; (37) Chavarria-K. 1985; (38) Cohen 1973; (39) Steenman & Thè 1989. (41) Cohen 1977; (42) Garmany 1973; (43) Knacke et al. 1973; (44) Chavarria-K. et al. 1988; (45) Wilson et al. 1970; (46) Herbst et al. 1982; (51) Finkenzeller 1985; (52) Panagia 1973; (54) Strom et al. 1972.

REFERENCES

Adams, F., Emerson, J., & Fuller, G. 1990, ApJ, 257, 606
Adams, F., Lada, C. J., & Shu, F. K. 1987, ApJ, 321, 788
Aitken, D. K., & Roche, P. F. 1981, MNRAS, 196, 39P
Allen, D. A. 1973, MNRAS, 161, 145
Allen, C. W. 1973, Astrophysical Quantities (3d ed.; London: Athlone)
Allen, D. A., Hyland, A. R., Longmore, A. J., Cashwell, J. L., Gross, W. M., & Haynes, R. F. 1977, ApJ, 217, 108
Altenhoff, W. J., Braes, L. L. E., Olnon, F. M., & Wendker, H. J. 1976, A&A, 46, 11
Aspin, C., McLean, I. S., & McCaughrean, M. J. 1985, A&A, 144, 220
Atlas of Low Resolution *IRAS* Spectra. 1986, *IRAS* Science Team, prepared by F. M. Olnon & E. Raimond (A&AS, 65, 607)
Aumann, H. H., et al. 1984, ApJ, 278, L23
Bastien, U., & Mundt, R. 1979, A&AS, 36, 57
Bastien, P. 1985, ApJS, 59, 277
Bastien, P., & Menard, F. 1990, ApJ, 364, 232
Bechis, K. P., Harvey, P. M., Campbell, M. F., & Hoffmann, W. F. 1978, ApJ, 226, 439
Beckwith, S. V. W., Sargent, A., Chini, R. S., & Gusten, R., 1990, AJ, 99, 924
Bergner, Y. K., et al. 1988, Astrophysics, 28(3), 313
Berrilli, F., Lorenzetti, D., Saraceno, P., & Strafella, F. 1987, MNRAS, 228, 833 (Paper I)
Bertout, C. 1989, ARA&A, 27, 351
Bieging, J. H., Cohen, M., & Schwartz, P. R. 1984, ApJ, 282, 699
Blaauw, A., Hiltner, W. A., & Johnson, H. L. 1959, ApJ, 130, 69; erratum 1959, ApJ, 131, 527
Boesono, B., Thè, P. S., & Tjin A Djie, H. R. E. 1987, Ap&SS, 137, 167
Bouchet, P., Manfroid, J., & Schmider, F. X. 1991, A&AS 91, 409
Bouchet, P., Moneti, A., Slezak, E., Le Bertre, T., & Manfroid, J. 1989, A&AS, 80, 379
Brandt, J. C., Stecher, T. P., Crawford, D. L., & Maran, S. P. 1971, ApJ, 163, L99
Braz, M. A., & Epchtein, N. 1982, A&A, 111, 91
Breger, M. 1974, ApJ, 188, 53
Brusaard, P. J., & Van de Hulst, H. C. 1962, Rev. Mod. Phys., 34, 507
Calvet, N., & Cohen, M. 1978, MNRAS, 182, 687
Cantó, J., Rodríguez, L. F., Barral, J. F., & Carral, P. 1981, ApJ, 244, 102
Cantó, J., Rodríguez, L. F., Calvet, N., & Levreault, R. M. 1984, ApJ, 282, 631
Catala, C. 1989, in Proc. ESO Workshop on Low Mass Star Formation and Pre-Main Sequence Objects, ed. B. Reipurth (Garching: ESO), 471
Chavarria-K., C. 1981, A&A, 101, 105
———. 1985, A&A, 148, 317
Chavarria-K., C., de Lara, E., Finkenzeller, U., Mendoza, E. E., & Ocegueda, J. 1988, A&A, 197, 15
Chernyshev, A. V., & Shevchenko, V. S. 1988, Astrophysics, 29(1), 439
Cohen, M. 1972, ApJ, 173, L61
———. 1973a, MNRAS, 161, 85
———. 1973b, MNRAS, 161, 97
———. 1973c, MNRAS, 161, 105
———. 1973d, MNRAS, 164, 395
———. 1974, MNRAS, 169, 257
———. 1977, ApJ, 215, 533
Cohen, M., & Barlow, M. J. 1975, Astrophys. Letters, 16, 165
Cohen, M., Bieging, J. H., & Schwartz, P. R. 1982, ApJ, 253, 707
Cohen, M., Emerson, J. P., & Beichman, C. A. 1989, ApJ, 339, 455
Cohen, M., Harvey, P. M., & Schwartz, R. D. 1985, ApJ, 296, 633
Cohen, M., & Kuhi, L. V. 1979, ApJS, 41, 743
Cohen, M., & Witteborn, F. C. 1985, ApJ, 294, 345
Curiel, S., Rodríguez, L. F., Cantó, J., Bohigas, J., Roth, M., & Torrelles, J. M. 1989, Ap. Letters Comm., 27, 299
Dachs, J., & Wamsteker, W. 1982, A&A, 107, 240
Dent, W. R. F., Sandell, G., Duncan, W. D., & Robson, E. I. 1989, MNRAS, 238, 1497
De Winter, D., & Thè, P. S. 1990, Ap&SS, 166, 99
Draine, B. T., & Lee, H. M. 1984, ApJ, 285, 89
Drissen, L., Bastien, P., & St.-Louis, N. 1989, AJ, 97, 814

Dyck, H. M., & Milkey, R. W. 1972, PASP, 81, 597
Edwards, S., Cabrit, S., Strom, S. E., Heyer, I., Strom, K. M., & Anderson, E. 1987, ApJ, 321, 473
Elias, J. H. 1978a, ApJ, 224, 453
———. 1978b, ApJ, 224, 857
Evans, N. J., II, Levreault, R. M., & Harvey, P. M. 1986, ApJ, 301, 894
Finkenzeller, U. 1985, A&A, 151, 340
Finkenzeller, U., & Mundt, R. 1984, A&AS, 55, 109
Garmany, C. D. 1973, AJ, 78, 185
Garrison, L. M., & Anderson, L. M. 1978, ApJ, 221, 601
Gehrz, R. D., Hackwell, J. A., & Jones, T. W. 1974, ApJ, 191, 675
Gezari, D. Y., Schmitz, M., & Mead, J. M. 1987, NASA Reference Publ. 1196 (2d ed.)
Glass, I. S., & Penston, M. V. 1974, MNRAS, 167, 237
Goodrich, R. W. 1986, ApJ, 311, 882
Gould, R. J. 1985, ApJ, 294, 23
———. 1986, ApJ, 302, 205
Güdel, M., Benz, A. O., Catala, C., & Praderie, F. 1989, A&A, 217, L9
Hamann, F., & Persson, S. E. 1989, ApJ, 339, 1078
Hartmann, L., Kenyon, S. J., Hewett, R., Edwards, S., Strom, K. M., Strom, S. E., & Stauffer, J. R. 1989, ApJ, 338, 1001
Harvey, P. M., Thronson, H. A., Jr., & Gatley, I. 1979, ApJ, 231, 115
Harvey, P. M., & Wilking, B. A. 1982, PASP, 94, 285
Herbig, G. H. 1957, ApJ, 125, 654
———. 1958, ApJ, 128, 259
———. 1960, ApJS, 4, 337
Herbig, G. H., & Bell, K. R. 1988, Lick Obs. Bull., 1111
Herbig, G. H., & Rao, N. K. 1972, ApJ, 174, 401
Herbst, W. 1975, AJ, 80, 863
Herbst, W., Holtzman, J. A., & Phelps, B. E. 1982, AJ, 87, 1710
Herbst, W., Miller, D. P., Warner, J. W., & Herzog, A. 1982, AJ, 87, 98
Hessman, F. V., Eisloffel, J., Mundt, R., Hartmann, L. W., Herbst, W., & Krautter, J. 1991, ApJ, 370, 384
Humphreys, R. M., Merrill, K. M., & Black, J. H. 1980, ApJ, 237, L17
IRAS Catalog and Atlases: Explanatory Supplement. 1985, ed. C. A. Beichman, G. Neugebauer, H. J. Habing, P. E. Clegg, & T. J. Chester (Washington, DC: GPO)
Jain, S. K., Bhatt, H. C., & Sagar, R. 1990, A&AS, 83, 237
Johnson, H. L. 1965, Comm. Lunar Planet Lab., 3, 73
Kataza, H., & Maihara, T. 1991, A&A, 248, L1
Kenyon, S. J., & Hartmann, L. 1987, ApJ, 323, 714
Knacke, R. F., Strom, K. M., Strom, S. E., Young, E., & Kunkel, W. 1973, ApJ, 179, 84
Koresko, C. D., Beckwith, S. V. W., & Sargent, A. 1989, AJ, 98, 1394
Lamers, H. J. G. L. M., & Waters, L. B. F. M. 1984, A&A, 136, 37
Lebofsky, M. J., Kleinmann, S. G., Rieke, G. H., & Low, F. J. 1976, ApJ, 206, L157
Leinert, C., Haas, M., & Lenzen, R. 1991, A&A, 246, 180
Lenzen, R. 1987, A&A, 173, 124
Levreault, R. M. 1988, ApJS, 67, 283
Lorenzetti, D., Saraceno, P., & Strafella, F. 1983, ApJ, 264, 554
Murdin, P., & Penston, M. V. 1977, MNRAS, 181, 657
Natta, A., Palla, F., Butner, H. M., Evans, N. J., II, & Harvey, P. M. 1992, ApJ, 391, 805
Palla, F., & Stahler, S. W. 1990, ApJ, 360, L47
———. 1991, ApJ, 375, 288
Panagia, N. 1973, AJ, 78, 929
Paresce, F., & Burrows, C. 1987, ApJ, 319, L23
Penston, M. V., Allen, D. A., & Lloyd, C. 1976, Observatory, 96, 22
Persson, S. E., McGregor, P. J., & Campbell, B. 1988, ApJ, 326, 339
Petrova, N. N., & Shevchenko, S. V. 1987, Sov. Astron. Lett., 13(4), 289
Poetzel, R., Mundt, R., & Ray, T. P. 1989, A&A, 224, L13
Racine, R. 1968, AJ, 73, 233
Ray, T. P., Poetzel, R., Solf, J., & Mundt, R. 1990, ApJ, 357, L45
Rieke, G. H., & Lebofsky, M. J. 1985, ApJ, 288, 618
Roche, P. F., Aitchen, D. K., & Smith, C. H. 1991, MNRAS, 252, 282
Rodríguez, L. F., Torrelles, J. M., & Moran, J. M. 1981, AJ, 86, 1245
Rydgren, A. E., & Vrba, F. J. 1987, PASP, 99, 482
Sandell, G., & Liseau, R. 1985, in Nearby Molecular Clouds, ed. G. Serra (Berlin: Springer-Verlag), 227
Scarrott, S. M., Draper, P. W., & Warren-Smith, R. F. 1989, MNRAS, 237, 621
Serkowsky, K. 1969, ApJ, 158, L107
Shevchenko, V. S., & Yakubov, S. D. 1989, Soviet Astron., 33, 370
Shirt, J. V., Warren-Smith, R. F., & Scarrott, S. M. 1983, MNRAS, 204, 1257
Shu, F. H., Adams, F. C., & Lizano, S. 1987, ARA&A, 25, 23
Simon, T. 1974, AJ, 79, 1047
Sitko, M. L. 1981, ApJ, 247, 1024
Skinner, S. L., Brown, A., & Linsky, J. L. 1990, ApJ, 357, L39
Smith, B. A., & Terrile, R. J. 1984, Science, 226, 1421
Sorrell, W. H. 1990, ApJ, 261, 150
Steenman, H., & Thè, P. S. 1989, Ap&SS, 161, 99
Strom, K. M., Strom, S. E., Edward, S., Cabrit, S., & Skrutskie, M. F. 1989, AJ, 97, 1451
Strom, S. E., Keene, J., Edwards, S., Hillenbrad, L., Strom, K. M., Gauvin, L., & Condon, G. 1991, in Angular Momentum Evolution of Young Stars, ed. S. Catalano & J. Stauffer (Dordrecht: Kluwer), 63
Strom, S. E., Strom, K. M., Brooke, A. L., Bregman, J., & Yost, J. 1972a, ApJ, 171, 267
Strom, S. E., Strom, K. M., Yost, J., Carrasco, L., & Grasdalen, G. 1972b, ApJ, 173, 353
Thè, P. S., Felenbok, P., Cuypers, H., & Tjin A Djie, H. R. E. 1985, A&A, 149, 42
Thè, P. S., Wesselius, P. R., Tjin A Djie, H. R. E., & Steenman, H. 1986, A&A, 155, 347
Tielens, A. G. G. M., & Hollenbach, D. 1985, ApJ, 291, 772
Volk, K., & Cohen, M. 1989, AJ, 98, 931
Vrba, F. J. 1975, ApJ, 195, 101
Vrba, F. J., Schmidt, G. D., & Hintzen, P. M. 1979, ApJ, 277, 185
Vrba, F. J., Strom, S. E., & Strom, K. M. 1976, ApJ, 81, 317
Ward-Thompson, D., Warren-Smith, R. F., Scarrott, S. M., & Wolstencroft, R. D. 1985, MNRAS, 215, 537
Warren-Smith, R. F., Scarrott, S. M., King, D. J., Taylor, K. N. R., Bingham, R. G., & Murdin, P. 1980, MNRAS, 192, 339
Weintraub, D. A. 1990, ApJS, 74, 575
Wilking, B. A., Harvey, P. M., Joy, M., Hyland, A. R., & Jones, T. J. 1985, ApJ, 293, 165
Wilking, B. A., Mundy, L. G., & Schwartz, R. D. 1986, ApJ, 303, L61
Williams, P. M., Beattie, D. H., & Stewart, J. M. 1977, MNRAS, 178, 619
Wilson, T. L., Mezger, P. G., Gardner, F. F., & Milne, D. K. 1970, A&A, 6, 364
Withcomb, S. E., Gatley, I., Hildebrand, R. H., Keene, J., Sellgren, K., & Werner, M. 1981, ApJ, 246, 416
Whittet, D. C. B., & Van Breda, I. G. 1980, MNRAS, 192, 467
Wolf, B., & Stahl, O. 1985, A&A, 148, 412